JOURNAL OF GUIDANCE, CONTROL, AND DYNAMICS
Vol. 40, No. 7, July 2017

Aerodynamic Three-Axis Attitude Stabilization of a Spacecraft by Center-of-Mass Shifting

Simone Chesi*
Naval Postgraduate School, Monterey, California 93943
Qi Gong†
University of California, Santa Cruz, Santa Cruz, California 95064
and
Marcello Romano‡
Naval Postgraduate School, Monterey, California 93943

DOI: 10.2514/1.G002460

This paper proposes a spacecraft attitude control technique based on the use of center-of-mass shifting. In particular, the position vector of the spacecraft's center of pressure with respect to the center of mass is modified by shifting masses, which results in a change of the aerodynamic torque vector within the plane perpendicular to the aerodynamic drag. This results in an underactuated control system. To achieve full three-axis stabilization, additional actuators (either a reaction wheel or a set of magnetic torquers) are considered. An adaptive nonlinear attitude regulation control law was designed in order to obtain an ideal control torque based on the Lyapunov method and its stability was proven by LaSalle's invariance principle. The control torque was then allocated to steer three shifting masses and either a reaction wheel or three magnetic torquers. Numerical simulations are reported, confirming the analytic results. The proposed method decreases the residual oscillation error typically associated with magnetic controlled attitude in the presence of residual aerodynamic torque. Therefore, it might contribute to achieve higher pointing accuracy of small spacecraft in low Earth orbit.

I. Introduction

TYPICAL attitude control systems for orbiting spacecraft are based on the use of three types of actuators [1]: mass expulsion devices, angular momentum exchange devices, and magnetic torquers [2]. Attitude control based upon the exploitation of the gravity gradient torque has also been studied and used [3], as well as passive attitude control based upon the exploitation of the residual aerodynamic torque [3–8].

The active use of the residual aerodynamic drag has been previously proposed and investigated for attitude maneuvering by using control surfaces [7,8], for orbital maneuvering [9–16], and for coupled orbital and attitude maneuvering by using the motion of a drag sail with regard to the spacecraft main body [17].

Furthermore, the dynamics and control of a spacecraft with moving masses have been previously extensively investigated. In particular, [18,19] studied the dynamic modeling of such a system, and [20] studied its application to orbital control with a focus on formation flight.

The effects of moving masses on the orientation of a spacecraft with a solar sail were investigated in [21–24]. In particular, [21] analyzed the dynamic model of a solar-sail spacecraft including internal moving masses and a gimbaled control boom. Reference [23] proposed a control system based on a two-axis gimbaled control boom to counteract the effect of the solar torque. Reference [24] presented an attitude control system based on two shifting masses for controlling the pitch and yaw motion of a solar sailcraft.

Another application of internal shifting masses regards the attitude control of spinning spacecraft. In particular, by using one shifting mass, [25] proposed to control the coning motion of a spinning spacecraft during orbital transfers; whereas [26,27] showed that a tumbling motion can be converted into a simple spin. Reference [28] studied the spinning stabilization of a spacecraft with two shifting masses driven by a linear quadratic regulator.

The effect of internal mass motion on the spacecraft attitude has also been considered to model the effect of fuel sloshing [29–31].

Finally, the use of shifting masses has been recently proposed to control the attitude of small spacecraft. In particular, [32] considered one shifting mass in a one-unit CubeSat. The nonlinear equations of motion were derived by using the Lagrangian approach and a linear controller was designed. Reference [33] considered the effect of two shifting masses on the orientation of a three-unit CubeSats. Notably, both [32,33] did not consider the effect of the aerodynamic torque. Control with moving masses of a spacecraft during reentry has been previously proposed in [34,35].

This paper proposes, for the first time to the best knowledge of the authors, to stabilize the attitude of a spacecraft by using shifting masses to actively control the residual aerodynamic torque. As it is well known, the aerodynamic torque about the center of mass can be considered equal to the moment with respect to the spacecraft center of mass of the residual aerodynamic drag vector as if it was applied to the center of pressure, which is a point dependent on the geometry and, in general, on the attitude of the spacecraft. As notionally shown in Fig. 1a and explained more in detail in the following, by shifting one mass m_i along a straight line with a displacement $d\underline{\boldsymbol{r}}_i$, the spacecraft center of mass (CM) is shifted along a parallel direction with a displacement $d\boldsymbol{r}_{\mathrm{CM}}$ given by

$$d\underline{\boldsymbol{r}}_{\mathrm{CM}} = \frac{m_i}{M} d\underline{\boldsymbol{r}}_i \tag{1}$$

where M is the total mass of the spacecraft. Consequently, the position vector of the spacecraft center of pressure (cp) with respect to the spacecraft center of mass changes from $\underline{\boldsymbol{r}}_{\mathrm{cp}}$ to $\underline{\boldsymbol{r}}'_{\mathrm{cp}} = \underline{\boldsymbol{r}}_{\mathrm{cp}} - d\underline{\boldsymbol{r}}_{\mathrm{CM}}$, and the aerodynamic torque $\underline{\boldsymbol{T}}_{\mathrm{aero}} = \underline{r}_{\mathrm{cp}} \times \underline{\boldsymbol{F}}_{\mathrm{aero}}$ has a variation

$$d\underline{\boldsymbol{T}}_{\mathrm{aero}} = (\underline{\boldsymbol{T}}'_{\mathrm{aero}} - \underline{\boldsymbol{T}}_{\mathrm{aero}}) = (\underline{r}'_{\mathrm{cp}} - \underline{r}_{\mathrm{cp}}) \times \underline{\boldsymbol{F}}_{\mathrm{aero}} = -d\underline{\boldsymbol{r}}_{\mathrm{CM}} \times \underline{\boldsymbol{F}}_{\mathrm{aero}} \tag{2}$$

Received 6 September 2016; revision received 18 January 2017; accepted for publication 20 February 2017; published online 25 May 2017.

*NRC Research Fellow, Mechanical and Aerospace Engineering Department; schesi@nps.edu. Member AIAA.
†Associate Professor, Department of Applied Mathematics and Statistics; qigong@soe.ucsc.edu.
‡Associate Professor, Mechanical and Aerospace Engineering Department; mromano@nps.edu. Associate Fellow AIAA.

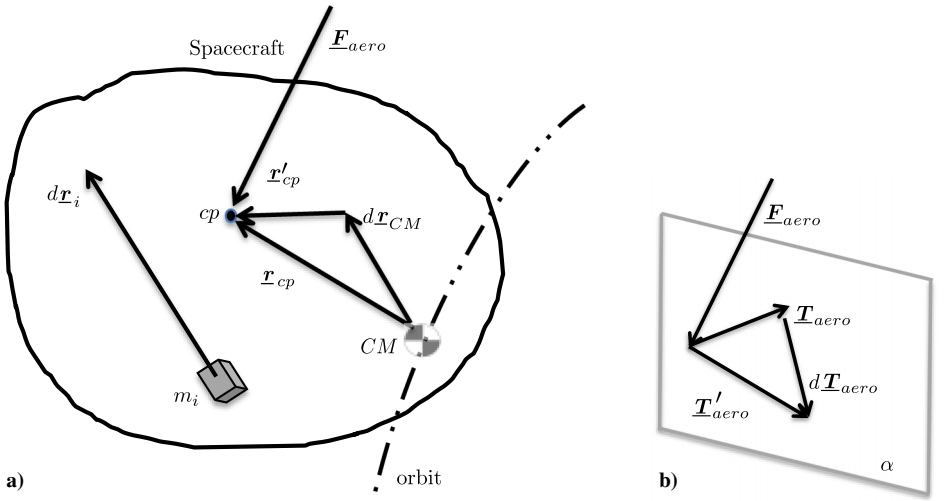

Fig. 1 Illustration of the basic concept of shifting masses on board a spacecraft in order to change the aerodynamic torque.

By neglecting aerodynamic lift, atmospheric corotation, thermal motion, and wind, the aerodynamic drag force $\underline{\boldsymbol{F}}_{\text{aero}}$ is directed parallel and opposite to the orbital velocity. Therefore, independently from the direction of the translation axis of m_i, the motion of the shifting mass can only generate a variation of the aerodynamic torque on a plane α perpendicular to the aerodynamic force $\underline{\boldsymbol{F}}_{\text{aero}}$ (as illustrated in Fig. 1b). To span the entire plane α, at least two shifting masses along two different axes are needed. However, in order to mitigate the possible occurrence of the direction of one shifting mass being parallel to the aerodynamic force, three shifting masses along three different axes are needed in order to ensure the ability of the control system to generate a torque that spans the entire plane α independently from the spacecraft attitude.

The exclusive use of shifting masses would lead to an underactuated system. To achieve full three-axis stabilization, an additional set of actuators able to generate a torque along the orbital velocity is here considered (either one reaction wheel or three magnetotorquers).

The control design was conducted in two steps. First, a nonlinear adaptive control law was formulated to stabilize the spacecraft attitude subjected to ideal actuators (unconstrained and fully actuating torque), starting from a generic initial condition in terms of the attitude and initial angular velocity toward a stable condition in which the body-fixed coordinate system was aligned with the orbital coordinate system. The designed control law was adaptive with respect to the position of the spacecraft center of mass, which was assumed to be unknown. The stability of this nonlinear adaptive control system was proven by the LaSalle's invariance principle [36]. Second, a torque steering logic (or control allocation algorithm) was designed in order to generate the torque determined by the aforementioned nonlinear adaptive control law by moving the shifting masses and commanding the additional actuators (either the reaction wheel or the three magnetotorquers), and therefore combining the subspace of the aerodynamic torque modulated by the shifting masses with the subspace of the torque generated by the other actuators.

During both steps of the control design, the spacecraft center of pressure was assumed to be known and not affected by the position of the shifting masses. The proposed method to exploit the residual aerodynamic torque to control a spacecraft is particularly advantageous for small spacecraft (e.g. nanosatellites [37]) and the proposed use of shifting masses coupled with magnetic control greatly decrease the residual oscillation error due to underactuation typically associated with magnetic controlled attitude of small spacecraft in presence of residual aerodynamic torque [6,37–42].

The paper is organized as follows. Section II introduces the model of the system. Section III presents the design of the adaptive attitude control law. Section IV introduces the control allocation of the shifting masses and the additional actuators. Section V reports the simulation results, and Sec. VI draws the conclusions.

II. System Modeling

A. Coordinate Systems

The following three Cartesian coordinate systems are here used: an inertial coordinate system ($\underline{\hat{\boldsymbol{X}}}^i$, $\underline{\hat{\boldsymbol{Y}}}^i$, $\underline{\hat{\boldsymbol{Z}}}^i$), an orbital coordinate system ($\underline{\hat{\boldsymbol{x}}}^o$, $\underline{\hat{\boldsymbol{y}}}^o$, $\underline{\hat{\boldsymbol{z}}}^o$), and a body-fixed coordinate system ($\underline{\hat{\boldsymbol{x}}}^b$, $\underline{\hat{\boldsymbol{y}}}^b$, $\underline{\hat{\boldsymbol{z}}}^b$). (In this paper, the underlined bold symbol is used to identify a Gibbsian vector, i.e., a quantity possessing magnitude, direction, and sense. A nonunderlined bold symbol is instead used to identify the column matrix of scalar components of a Gibbsian vector in a particular coordinate system.) The three coordinate systems are shown in Fig. 2. The inertial coordinate system has its origin in the Earth's center. The orbital coordinate system has its origin in the spacecraft's center of mass identified by the vector $\underline{\boldsymbol{R}}_{\text{CM}}$ with respect to the Earth's center), with the $\underline{\hat{\boldsymbol{x}}}^o$ axis pointing along the instantaneous orbital velocity, the $\underline{\hat{\boldsymbol{z}}}^o$ axis pointing toward the nadir, and the $\underline{\hat{\boldsymbol{y}}}^o$ axis completing the right triad. The body-fixed coordinate system has its origin in a particular point A of the spacecraft, as described in Sec. II.C, with the axes being the principal axes of inertia for that particular point.

The following hypothesis is assumed:

Hypothesis 1: The spacecraft is in a circular orbit around the Earth.

Therefore, the linear velocity $\underline{\boldsymbol{\nu}}^o_{\text{CM}}$ and angular velocity $\underline{\boldsymbol{\omega}}^o_{oi}$ have constant magnitude and can be written in scalar components in the orbital coordinate system as

$$\boldsymbol{\nu}^o_{\text{CM}} = \sqrt{\frac{\mu}{R_{\text{CM}}}}\begin{bmatrix}1\\0\\0\end{bmatrix}, \quad \text{and} \quad \boldsymbol{\omega}^o_{oi} = \sqrt{\frac{\mu}{R^3_{\text{CM}}}}\begin{bmatrix}0\\-1\\0\end{bmatrix} \tag{3}$$

where R_{CM} is the radius of the orbit, and μ is the gravitational parameter of the Earth (equal to the gravitational constant times the Earth's mass).

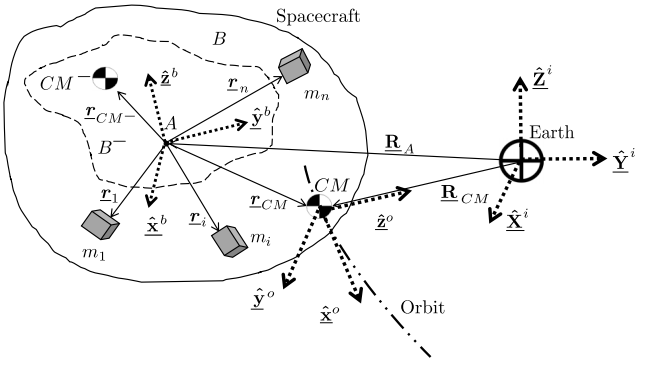

Fig. 2 Notional illustration of an orbiting spacecraft with shifting masses.

B. Spacecraft Attitude Kinematics

The orientation of the body-fixed coordinate systems with respect to the inertial coordinate system can be described by the orientation quaternion $\boldsymbol{q}_{bi}(\boldsymbol{\eta}, \xi) \in \mathbb{R}^4$ [3,43]:

$$\boldsymbol{q}_{bi} = \begin{bmatrix} \boldsymbol{\eta} \\ \xi \end{bmatrix}, \qquad \eta = \begin{bmatrix} \eta_1 \\ \eta_2 \\ \eta_3 \end{bmatrix} \sin\left(\frac{\phi}{2}\right), \qquad \xi = \cos\left(\frac{\phi}{2}\right) \tag{4}$$

subjected to the constraint

$$\boldsymbol{\eta}^T\boldsymbol{\eta} + \xi^2 = 1 \tag{5}$$

where $\boldsymbol{\eta} \in \mathbb{R}^3$ and $\xi \in \mathbb{R}$ are the imaginary and real parts of the quaternion $\boldsymbol{q}$, respectively. The terms $(\eta_1\eta_2\eta_3)$ are the components of the unit vector $\boldsymbol{\eta}$ along the eigenaxis of rotation, and ϕ is the magnitude of the rotation around this vector.

The quaternion satisfies the differential equation [44]

$$\begin{aligned} \dot{\boldsymbol{\eta}} &= \frac{1}{2}(\boldsymbol{\eta}^{\times}\boldsymbol{\omega} + \xi\boldsymbol{\omega}) \\ \dot{\xi} &= -\frac{1}{2}\boldsymbol{\omega}^T\boldsymbol{\eta} \end{aligned} \tag{6}$$

where $\boldsymbol{\omega} \in \mathbb{R}^3$ is the angular velocity of the body-fixed coordinate system with respect to the inertial coordinate system expressed in the body-fixed coordinate system. The direction cosine matrix (DCM) $\boldsymbol{R}(\boldsymbol{\eta}, \xi)_{bi} \in \mathbb{R}^{3\times3}$, from the inertial coordinate system to the body-fixed coordinate system is defined as [45]

$$\boldsymbol{R}(\boldsymbol{\eta}, \xi)_{bi} = (\xi^2 - \boldsymbol{\eta}^T\boldsymbol{\eta})I_{3\times3} + 2\boldsymbol{\eta}\boldsymbol{\eta}^T - 2\xi[\boldsymbol{\eta}^{\times}] \tag{7}$$

where $[\boldsymbol{\eta}^{\times}] \in \mathbb{R}^{3\times3}$ is used to express the cross product in matrix form

$$[\boldsymbol{\eta}^{\times}] = \begin{bmatrix} 0 & -\eta_3 & \eta_2 \\ \eta_3 & 0 & -\eta_1 \\ -\eta_2 & \eta_1 & 0 \end{bmatrix} \tag{8}$$

The quaternion $\boldsymbol{q}_{oi}(\boldsymbol{\eta}_o, \xi_0)$ satisfies the differential equations

$$\dot{\boldsymbol{\eta}}_o = \frac{1}{2}(\boldsymbol{\eta}_o\boldsymbol{\omega}^o_{oi} + \xi_o\boldsymbol{\omega}^o_{oi}) \quad \dot{\xi}_o = -\frac{1}{2}(\boldsymbol{\omega}^o_{oi})^T\boldsymbol{\eta}_o \tag{9}$$

The DCM from the inertial to the orbital coordinate system is defined by

$$\boldsymbol{R}(\boldsymbol{\eta}_o, \xi_o)_{oi} = (\xi_o^2 - \boldsymbol{\eta}_o^T\boldsymbol{\eta}_o)I_{3\times3} + 2\boldsymbol{\eta}_o\boldsymbol{\eta}_o^T - 2\xi_o[\boldsymbol{\eta}_o^{\times}] \tag{10}$$

The attitude error DCM from the orbital coordinate system to the body-fixed coordinate system is given by

$$\boldsymbol{R}_{bo} = \boldsymbol{R}_{bi}\boldsymbol{R}_{oi}^T = (\xi_e^2 - \boldsymbol{\eta}_e^T\boldsymbol{\eta}_e)I_{3\times3} + 2\boldsymbol{\eta}_e\boldsymbol{\eta}_e^T - 2\xi_e[\boldsymbol{\eta}_e^{\times}] \tag{11}$$

where

$$\begin{aligned} \boldsymbol{\eta}_e &= \xi_o\boldsymbol{\eta} - \xi\boldsymbol{\eta}_o + [\boldsymbol{\eta}^{\times}]\boldsymbol{\eta}_o \\ \xi_e &= \xi\xi_o + \eta^T\eta_o \end{aligned} \tag{12}$$

composes the quaternion error $\boldsymbol{q}_e = \boldsymbol{q}_{bo}(\boldsymbol{\eta}, \xi)$, which satisfies the differential equations

$$\begin{aligned} \dot{\boldsymbol{\eta}}_e &= \frac{1}{2}(\boldsymbol{\eta}_e^{\times}\boldsymbol{\omega}_{bo} + \xi_e\boldsymbol{\omega}_{bo}) \\ \dot{\xi}_e &= -\frac{1}{2}\boldsymbol{\omega}_{bo}^T\eta_e \end{aligned} \tag{13}$$

Furthermore, it results in

$$\boldsymbol{\omega} = \boldsymbol{\omega}_{bo} + \boldsymbol{R}_{bo}\boldsymbol{\omega}^o_{oi} \tag{14}$$

and, by taking the time derivative,

$$\dot{\boldsymbol{\omega}} = \dot{\boldsymbol{\omega}}_{bo} + \dot{\boldsymbol{R}}_{bo}\boldsymbol{\omega}^o_{oi} + \boldsymbol{R}_{bo}\dot{\boldsymbol{\omega}}^o_{oi} \tag{15}$$

Because the orbit is circular, the last term on the right-hand side of Eq. (15) is zero; by taking into account the Darboux theorem, it yields

$$\dot{\boldsymbol{\omega}} = \dot{\boldsymbol{\omega}}_{bo} - \boldsymbol{\omega}^{\times}_{bo}\boldsymbol{R}_{bo}\boldsymbol{\omega}^o_{oi} \tag{16}$$

C. Model of the Attitude Dynamics of a Spacecraft with Shifting Masses

A spacecraft system B having n shifting masses m_i with $i = 1, \ldots, n$ is considered. The spacecraft system B can be seen as the union of two portions: a body B^- encompassing the spacecraft body without the shifting masses, and the set of the n shifting masses (see Fig. 2). The center of mass of the system portion B^- is at CM^-, whereas the center of mass of the whole system B is at the CM.

The following main simplifying hypotheses are assumed:

Hypothesis 2: The body B^- is rigid.

Hypothesis 3: Each shifting mass is a point mass.

Hypothesis 4: Each shifting mass can move only along a straight line relative to the spacecraft body.

Hypothesis 5: A point A exists that is the intersection of the lines of motion of the n masses.

Hypothesis 6: The gravitational acceleration is considered uniform over the spacecraft and equal to the one at the location of the center of mass of the spacecraft (i.e., the gravity gradient is neglected).

Hypothesis 7: The variation of the dyadic of inertia due to the change in position of the shifting masses is neglected.

Hypothesis 8: The shifting masses' displacement, relative velocity, and acceleration have relatively small magnitude with respect to the other characteristic quantity of the system.

The spacecraft mass M can be expressed as

$$M = M^- + \sum_{i=1}^{n} m_i \tag{17}$$

where M^- is the mass of the spacecraft portion B^-.

The absolute angular momentum vector of the body B^- with respect to point A is, by definition ([39] p. 409),

$$\underline{\boldsymbol{\Gamma}}^A_{B^-} = \int_{B^-} \underline{\boldsymbol{r}} \times \underline{\dot{\boldsymbol{r}}}\, \mathrm{d}m = \int_{B^-} \underline{\boldsymbol{r}} \times \underline{\boldsymbol{\omega}} \times \underline{\boldsymbol{r}} = \underline{\underline{\boldsymbol{J}}}^A_{B^-} \cdot \underline{\boldsymbol{\omega}} \tag{18}$$

where $\underline{\boldsymbol{r}}$ is the position vector from point A to a differential element of mass dm; the dot symbol over a vector is used to indicate the time derivative of that vector evaluated in the inertial frame; $\underline{\boldsymbol{\omega}}$ is the angular velocity of the body B^- (and of B) with respect to the inertial frame; and

$$\underline{\underline{\boldsymbol{J}}}^A_{B^-} = \int_{B^-} (\underline{\boldsymbol{r}} \cdot \underline{\boldsymbol{r}}\, \underline{\underline{\boldsymbol{U}}} - \underline{\boldsymbol{r}}\, \underline{\boldsymbol{r}})\, \mathrm{d}m \tag{19}$$

is the inertia dyadic of the body B^- with respect to the point A, where $\underline{\underline{\boldsymbol{U}}}$ is the unit dyadic and $\underline{\boldsymbol{r}}\,\underline{\boldsymbol{r}}$ indicates a dyad (see, for instance, [45] p. 419). In writing Eq. (18), it has been taken into account that

$$\underline{\dot{\boldsymbol{r}}} = \mathring{\underline{\boldsymbol{r}}} + \underline{\boldsymbol{\omega}} \times \underline{\boldsymbol{r}} \tag{20}$$

where the circle symbol over a vector is used to indicate the time derivative of that vector evaluated in the spacecraft-body-fixed frame. Notably, $\mathring{\underline{\boldsymbol{r}}} = 0$ because of Hypothesis 2.

The absolute angular momentum vector of the set of shifting masses with respect to point A is, by definition ([45] p. 409),

$$\underline{\boldsymbol{\Gamma}}_m^A = \sum_{i=1}^{n} \underline{\boldsymbol{r}}_i \times m_i \dot{\underline{\boldsymbol{r}}}_i = \sum_{i=1}^{n} \underline{\boldsymbol{r}}_i \times m_i \dot{\underline{\boldsymbol{r}}}_i = \sum_{i=1}^{n} \underline{\boldsymbol{r}}_i \times \underline{\boldsymbol{\omega}} \times \underline{\boldsymbol{r}}_i = \sum_{i=1}^{n} \underline{\boldsymbol{r}}_i \times \underline{\boldsymbol{\omega}} \times \underline{\boldsymbol{r}}_i \tag{21}$$

where it has been taken into account that

$$\sum_{i=1}^{n} \underline{\boldsymbol{r}}_i \times m_i \dot{\underline{\boldsymbol{r}}}_i = 0$$

because the vectors $\underline{\boldsymbol{r}}$ and $\underline{\boldsymbol{r}}$ are parallel in accordance with Hypothesis 4.

Therefore, by taking into account Eqs. (18) and (21), the absolute momentum of the entire spacecraft B with respect to point A results in

$$\underline{\boldsymbol{\Gamma}}^A = \underline{\boldsymbol{\Gamma}}_{B^-}^A + \underline{\boldsymbol{\Gamma}}_m^A = \underline{\underline{\boldsymbol{J}}}^A \cdot \underline{\boldsymbol{\omega}} \tag{22}$$

where

$$\underline{\underline{\boldsymbol{J}}}^A = \underline{\underline{\boldsymbol{J}}}_{B^-}^A - \sum_{i=1}^{n} (\underline{\boldsymbol{r}}_i \cdot \underline{\boldsymbol{r}}_i \underline{\underline{\boldsymbol{U}}} - \underline{\boldsymbol{r}}_i \underline{\boldsymbol{r}}_i) \tag{23}$$

is the inertia dyadic of the entire spacecraft with respect to A.

The vectorial equation of rotational motion of the system can be written as ([45] p. 410)

$$\dot{\underline{\boldsymbol{\Gamma}}}^A = \underline{\boldsymbol{T}}^A + M \ddot{\underline{\boldsymbol{R}}}_A \times \underline{\boldsymbol{r}}_{\mathrm{CM}} \tag{24}$$

where $\underline{\boldsymbol{R}}_A$ is the position vector of point A with respect to any inertially fixed point (in particular, e.g., the Earth's center), and $\underline{\boldsymbol{T}}^A$ is the moment resultant with respect to A of all differential forces acting on the system.

Without losing generality, it is possible to write that (see Fig. 2)

$$\underline{\boldsymbol{R}}_A = \underline{\boldsymbol{R}}_{\mathrm{CM}} - \underline{\boldsymbol{r}}_{\mathrm{CM}} \rightarrow \ddot{\underline{\boldsymbol{R}}}_A = \ddot{\underline{\boldsymbol{R}}}_{\mathrm{CM}} - \ddot{\underline{\boldsymbol{r}}}_{\mathrm{CM}} \tag{25}$$

Furthermore, it is

$$M \ddot{\underline{\boldsymbol{R}}}_{\mathrm{CM}} = \underline{\boldsymbol{F}} \tag{26}$$

where $\underline{\boldsymbol{F}}$ is the force resultant of all external forces applied to the system.

It is useful to write

$$\underline{\boldsymbol{F}} = \underline{\boldsymbol{F}}_{\mathrm{gravity}} + \underline{\boldsymbol{F}}_{\mathrm{other}} \tag{27}$$

$$\underline{\boldsymbol{T}}^A = \underline{\boldsymbol{T}}_{\mathrm{gravity}}^A + \underline{\boldsymbol{T}}_{\mathrm{other}}^A \tag{28}$$

where the subindex gravity is used to indicate the actions resultant of the gravitational attraction, and the subindex other is used to indicate all other external resultant actions.

Furthermore, because of Hypothesis 6, it yields

$$\underline{\boldsymbol{F}}_{\mathrm{gravity}} = -\frac{\mu M}{R_{\mathrm{CM}}^3} \underline{\boldsymbol{R}}_{\mathrm{CM}} \tag{29}$$

$$\underline{\boldsymbol{T}}_{\mathrm{gravity}}^A = -\int_B \underline{\boldsymbol{r}} \, \mathrm{d}m \times \frac{\mu}{R_{\mathrm{CM}}^3} \underline{\boldsymbol{R}}_{\mathrm{CM}} = -\underline{\boldsymbol{r}}_{\mathrm{CM}} \times \frac{\mu M}{R_{\mathrm{CM}}^3} \underline{\boldsymbol{R}}_{\mathrm{CM}} \tag{30}$$

By substituting Eqs. (25–30) into Eq. (24), the vectorial equation of rotational motion for system B becomes

$$\dot{\underline{\boldsymbol{\Gamma}}}^A = \underline{\boldsymbol{T}}_{\mathrm{other}}^A + \underline{\boldsymbol{F}}_{\mathrm{other}} \times \underline{\boldsymbol{r}}_{\mathrm{CM}} - M \ddot{\underline{\boldsymbol{r}}}_{\mathrm{CM}} \times \underline{\boldsymbol{r}}_{\mathrm{CM}} \tag{31}$$

From Eq. (22), by taking into account that $\dot{\underline{\underline{\boldsymbol{J}}}}^A = \underline{\underline{0}}$ because of Hypothesis 7, it yields

$$\dot{\underline{\boldsymbol{\Gamma}}}^A = \dot{\underline{\boldsymbol{\Gamma}}}^A + \underline{\boldsymbol{\omega}} \times \underline{\boldsymbol{\Gamma}}^A = \underline{\underline{\boldsymbol{J}}}^A \cdot \dot{\underline{\boldsymbol{\omega}}} + \underline{\boldsymbol{\omega}} \times \underline{\underline{\boldsymbol{J}}}^A \cdot \underline{\boldsymbol{\omega}} \tag{32}$$

Furthermore, it yields

$$\underline{\boldsymbol{r}}_{\mathrm{CM}} = \frac{M^- \underline{\boldsymbol{r}}_{\mathrm{CM}^-} + \sum_{i=1}^{n} m_i \underline{\boldsymbol{r}}_i}{M} \tag{33}$$

By introducing Eqs. (32) and (33) into Eq. (31) and by taking into account that, because of Hypothesis 8, it is possible to neglect the term $M \ddot{\underline{\boldsymbol{r}}}_{\mathrm{CM}} \times \underline{\boldsymbol{r}}_{\mathrm{CM}}$ [23,24], the vector equation of motion finally becomes

$$\underline{\underline{\boldsymbol{J}}}^A \cdot \dot{\underline{\boldsymbol{\omega}}} = -\underline{\boldsymbol{\omega}} \times \underline{\underline{\boldsymbol{J}}}^A \cdot \underline{\boldsymbol{\omega}} + \underline{\boldsymbol{T}}_{\mathrm{other}}^A + \underline{\boldsymbol{F}}_{\mathrm{other}} \times \frac{M^- \underline{\boldsymbol{r}}_{\mathrm{CM}^-}}{M} + \underline{\boldsymbol{F}}_{\mathrm{other}} \frac{\sum_{i=1}^{n} m_i \underline{\boldsymbol{r}}_i}{M} \tag{34}$$

By projecting all dyadics and vectors along the body-fixed coordinate system, vectorial equation (34) can be written in the following equivalent matrix form, which will be used for further development in the next sections of the paper:

$$\boldsymbol{J}\dot{\boldsymbol{\omega}} = -\boldsymbol{\omega}^{\times} \boldsymbol{J}\boldsymbol{\omega} + \boldsymbol{T}_{\mathrm{other}}^A + \boldsymbol{F}_{\mathrm{other}}^{\times} \left(\frac{M^-}{M} \right) \boldsymbol{r}_{\mathrm{CM}^-} + \boldsymbol{F}_{\mathrm{other}}^{\times} \frac{\sum_{i=1}^{n} m_i \boldsymbol{r}_i}{M} \tag{35}$$

where $\boldsymbol{J}$ is indicating the inertia matrix with respect to A, and the other symbols have obvious meaning.

Equation (35) describes the system's dynamics and the coupling effect of the external forces related to the positions of the shifting masses.

D. Model of Aerodynamic Force and Torque on a Spacecraft with Shifting Masses

The following hypotheses are assumed:

Hypothesis 9: The spacecraft boundary is convex and composed of flat faces.

Hypothesis 10: The aerodynamic lift, atmospheric corotation, thermal motion, and wind are neglected.

Then, based on the results in [46], the column matrix of scalar components in the body-fixed coordinate system of the aerodynamic force over each of the p flat faces of area $S_i \in \mathbb{R}$ of the spacecraft can be modeled by the following equation:

$$\boldsymbol{F}_{di} = -\frac{1}{2} C_D \rho(h) \| \boldsymbol{v}_{\mathrm{s/c}} \|^2 \hat{\boldsymbol{n}}_i^T \hat{\boldsymbol{v}}_{\mathrm{s/c}} \hat{\boldsymbol{v}}_{\mathrm{s/c}} Si, \quad \text{for } = 1, 2, \ldots, p \tag{36}$$

where $C_D \in \mathbb{R}$ is the aerodynamic drag coefficient, and $\hat{\boldsymbol{n}}_i \in \mathbb{R}^3$ is the outward normal direction to the ith surface in body-fixed coordinate system. The atmospheric density, indicated by $\rho(h)$, is a function of the altitude [47]. The spacecraft velocity in the body-fixed coordinate system, denoted by $\hat{\boldsymbol{v}}_{\mathrm{s/c}} \in \mathbb{R}^3$, is given by

By defining

$$\boldsymbol{v}_{\mathrm{s/c}} = \boldsymbol{R}_{bo} v_o^o, \quad \text{and} \quad \hat{\boldsymbol{v}}_{\mathrm{s/c}} = \frac{\boldsymbol{v}_{\mathrm{s/c}}}{\| \boldsymbol{v}_{\mathrm{s/c}} \|} \tag{37}$$

$$k_d = -\frac{1}{2} C_D \rho \| \boldsymbol{v}_{\mathrm{s/c}} \|^2, \quad \text{and} \quad \chi_i = (\hat{\boldsymbol{n}}_i^T \boldsymbol{v}_{\mathrm{s/c}}) \tag{38}$$

Equation (36) can be written more compactly as

$$\boldsymbol{F}_{di} = k_d \chi_i \hat{\boldsymbol{v}}_{\mathrm{s/c}} S_i, \quad \text{for } i = 1, 2, \ldots, p \tag{39}$$

Assume the following hypothesis:

Hypothesis 11: The aerodynamic force and moment are the only external disturbance actions acting on the spacecraft.

Then, it results in

$$\boldsymbol{F}_{\text{other}} = \boldsymbol{F}_{\text{aero}} = \sum_{i=1}^{p} \boldsymbol{F}_{d_i}\delta_i = k_d\left[\sum_{i=1}^{p}(\chi_i S_i \delta_i)\right]\hat{\boldsymbol{v}}_{\text{s/c}} \tag{40}$$

where the function δ_i is defined as

$$\delta_i: \begin{cases} \delta_i = 1, & \chi_i > 0 \\ \delta_i = 0, & \chi_i \leq 0 \end{cases} \tag{41}$$

If $\chi_i \leq 0$, the ith side is shadowed with respect to the relative residual-atmosphere flow; therefore, it does not contribute to the aerodynamic force.

Furthermore, the aerodynamic moment with respect to A due to the distributed aerodynamic forces acting on the surface of the spacecraft results in

$$\boldsymbol{T}^A_{\text{other}} = \boldsymbol{T}^A_{\text{aero}} = \sum_{i=1}^{p}(r^{\times}_{\text{cp}}\boldsymbol{F}_{di}\delta_i) = k_d\left[\sum_{i=1}^{p}(\chi_i S_i \delta_i)\boldsymbol{r}_{\text{cp}_i}\right]^{\times}\hat{\boldsymbol{v}}_{\text{s/c}} \tag{42}$$

where $\boldsymbol{r}_{\text{cp}_i} \in \mathbb{R}^3$ indicates the column matrix of scalar components in the body-fixed coordinate system of the position vector of the center of pressure of the ith face with respect to A (e.g., equivalent to the geometric center for rectangular surfaces).

Alternatively to Eq. (42) the aerodynamic moment of the distributed aerodynamic forces with respect to A can be expressed as the moment with respect to A of the total aerodynamic force passing through the overall center of pressure of the spacecraft, i.e., as

$$\boldsymbol{T}^A_{\text{aero}} = \boldsymbol{r}^{\times}_{\text{cp}}\boldsymbol{F}_{\text{aero}} \tag{43}$$

where $\boldsymbol{r}_{\text{cp}} \in \mathbb{R}^3$ indicates the column matrix of scalar components of the position vector of the overall center of pressure with respect to A. By substituting the expression of $\boldsymbol{T}^A_{\text{aero}}$ from Eq. (43) into Eq. (42), and by taking into account Eq. (40), it yields

$$r_{\text{cp}} = \frac{\sum_{i=1}^{p}(\chi_i S_i \delta_i) r_{\text{cp}_i}}{\sum_{i=1}^{p}(\chi_i S_i \delta_i)} \tag{44}$$

By substituting Eqs. (40) and (42) into Eq. (35), the equations of motions become

$$\boldsymbol{J} = -\boldsymbol{\omega}^{\times}\boldsymbol{J}\boldsymbol{\omega} + \boldsymbol{\tau}_{\text{CM}^-} + \boldsymbol{\tau}_M + \boldsymbol{\tau}_{\text{cp}} \tag{45}$$

where it has been defined as

$$\begin{aligned}
\boldsymbol{\tau}_{\text{CM}^-} &= \boldsymbol{F}^{\times}_{\text{aero}}\left(\frac{M^-}{M}\right)\boldsymbol{r}_{\text{CM}^-} = k_d\left(\frac{M^-}{M}\right)\left[\sum_{i=1}^{p}(\chi_i S_i \delta_i)\right]\hat{\boldsymbol{\nu}}^{\times}_{\text{s/c}}\boldsymbol{r}_{\text{CM}^-} \\
&= K_{\text{CM}^-}\boldsymbol{r}^{\times}_{\text{CM}^-}\hat{\boldsymbol{\nu}}^{\times}_{\text{s/c}} \\
\boldsymbol{\tau}_M &= \boldsymbol{F}^{\times}_{\text{aero}}\frac{\sum_{i=1}^{n} m_i \boldsymbol{r}_i}{M} = \frac{k_d}{M}\left[\sum_{i=1}^{p}(\chi_i S_i \delta_i)\right]\left(\sum_{i=1}^{n} m_i r_i\right)^{\times}\hat{\boldsymbol{\nu}}_{\text{s/c}} \\
&= \frac{K_{\text{CM}^-}}{M^-}\left(\sum_{i=1}^{n} m_i r_i\right)^{\times}\hat{\boldsymbol{\nu}}_{\text{s/c}} \\
\boldsymbol{\tau}_{\text{cp}} &= \boldsymbol{T}^A_{\text{aero}} = k_d\boldsymbol{r}^{\times}_{\text{cp}}\hat{\boldsymbol{\nu}}_{\text{s/c}}
\end{aligned} \tag{46}$$

where it has been defined as

$$K_{\text{CM}-} = -K_d\left(\frac{M^-}{M}\right)\left[\sum_{i=1}^{p}(\chi_i S_i \delta_i)\right] \tag{47}$$

and where $\boldsymbol{\tau}_{\text{CM}^-}$ indicates the column matrix of the portion of the aerodynamic moment with respect to A, which is dependent on the position of the point CM^-, which is considered to be unknown and it is not a function of the position of the shifting masses. Furthermore, $\boldsymbol{\tau}_M$ indicates the column matrix of the portion of the aerodynamic moment with respect to A, which is dependent on the position of the shifting masses. Finally, $\boldsymbol{\tau}_{\text{cp}}$ indicates the column matrix of scalar components of the portion of the aerodynamic moment with respect to A, which is dependent on the position of the center of pressure, which is a function of the orientation of the spacecraft through the values of χ_i and δi, but it is not a function of the position of the shifting masses.

Notably, $\boldsymbol{\tau}_{\text{cp}}$ is the aerodynamic moment with respect to A due to the aerodynamic force considered passing through the center of pressure, whereas $\boldsymbol{\tau}_{\text{CM}^-}$ and $\boldsymbol{\tau}_M$ are the aerodynamic moment with respect to A due to the aerodynamic force considered passing through the spacecraft center of mass, and they are present in the equations of motions because of the (here) convenient choice of considering the pole of the angular momentum to be in A.

From the second equation in Eq. (46), it is clear that the aerodynamic moment $\boldsymbol{\tau}_M$ is a function of the cross product between the position of the shifting masses and the orbital velocity vector. Therefore, $\boldsymbol{\tau}_M$ is always on a plane perpendicular to the orbital velocity vector. Therefore, additional actuators are needed in order to generate a component of control torque along the orbital velocity vector, and thus to achieve full control of the spacecraft attitude.

III. Design of Ideal Control Torque Based on Nonlinear Adaptive Regulation Law

The control design is divided into two steps. First, an ideal control torque with respect to A, named $\boldsymbol{\tau}_t \in \mathbb{R}^3$ and spanning the three-dimensional space, is considered instead of the torque $\boldsymbol{\tau}_M$, which only spans a plane perpendicular to the orbital velocity. A control law is designed in this section for the ideal control torque; its stability is proven, and its convergence properties are studied.

Second, through a control allocation algorithm, the ideal control torque is generated by steering the shifting masses and additional actuators (either one reaction wheel or three magnetic torquers), as explained in Sec. IV.

By substituting $\boldsymbol{\tau}_M$ with $\boldsymbol{\tau}_t$, Eq. (45) becomes

$$\boldsymbol{J} = -\boldsymbol{\omega}^{\times}\boldsymbol{J}\boldsymbol{\omega} + \boldsymbol{\tau}_{\text{CM}^-} + \boldsymbol{\tau}_t + \boldsymbol{\tau}_{\text{cp}} \tag{48}$$

The design is here described of a nonlinear adaptive regulation control law to ensure the closed-loop stability for a spacecraft system having dynamics governed by Eq. (48) and driven by the ideal control torque $\boldsymbol{\tau}_t$. The control aims to regulate the attitude of the spacecraft toward the condition $\boldsymbol{q}_e = [0 \quad 0 \quad 0]^T$, i.e., the nadir-pointing condition with the body coordinate system superimposed to the orbital coordinate system, with $\boldsymbol{\omega}_{bo} = 0$. The authors have previously used a similar nonlinear adaptive control design for the automatic mass balance of a spacecraft three-axis simulator [48].

An adaptive control law is desired to handle the fact that the position $\boldsymbol{r}_{\text{CM}^-}$ of the center of mass of the spacecraft portion B^- (spacecraft without the shifting masses) is considered to be unknown, By defining the unknown parameter to be $\boldsymbol{\Theta} = r_{\text{CM}^-}$, the portion of the aerodynamic moment influenced by the position of CM^- can be rewritten as [see Eq. (46)]

$$\boldsymbol{\tau}_{\text{CM}^-} = K_{\text{CM}^-}(-\hat{\boldsymbol{v}}^{\times}_{\text{s/c}}\boldsymbol{r}_{\text{CM}^-}) = \boldsymbol{\Phi}\boldsymbol{\Theta}$$

where it is defined as

$$\boldsymbol{\Phi}(\boldsymbol{q}_e) = -K_{\text{CM}^-} - \hat{\boldsymbol{v}}^{\times}_{\text{s/c}} \tag{49}$$

Let $\hat{\boldsymbol{\Theta}}(t)$ be the estimation of the unknown parameter $\boldsymbol{\Theta}$, and let $\tilde{\boldsymbol{\Theta}}(t)$ be the estimation error, i.e.,

$$\tilde{\boldsymbol{\Theta}}(t) = \boldsymbol{\Theta} - \hat{\boldsymbol{\Theta}}(t) \tag{50}$$

Notably, it is

$$\dot{\tilde{\boldsymbol{\Theta}}} = -\dot{\hat{\boldsymbol{\Theta}}} \tag{51}$$

By using Eqs. (14) and (16), Eq. (48) can be expressed as a function of the angular velocity of the spacecraft with respect to the orbital frame as

$$\boldsymbol{J}(\dot{\boldsymbol{\omega}}_{bo}-\boldsymbol{\omega}_{bo}^{\times}\boldsymbol{\omega}_{oi})=-(\boldsymbol{\omega}_{bo}+\boldsymbol{\omega}_{oi})\times\boldsymbol{J}(\boldsymbol{\omega}_{bo}+\boldsymbol{\omega}_{oi})+\boldsymbol{\Phi}\boldsymbol{\Theta}+\boldsymbol{\tau}_t+\boldsymbol{\tau}_{\text{cp}} \tag{52}$$

where it has been defined as $\boldsymbol{\omega}_{oi}=\boldsymbol{R}_{bo}\boldsymbol{\omega}_{oi}^{o}$.

By combining Eqs. (52) and (13), the system dynamics and kinematics are expressed as

$$\begin{aligned}\dot{\boldsymbol{\omega}}_{bo}&=\boldsymbol{\omega}_{bo}^{\times}\boldsymbol{\omega}_{oi}+\boldsymbol{J}^{-1}(-(\boldsymbol{\omega}_{bo}+\omega_{oi})\times\boldsymbol{J}(\boldsymbol{\omega}_{bo}+\boldsymbol{\omega}_{oi})+\boldsymbol{\Phi}\boldsymbol{\Theta}+\tau_t+\tau_{\text{cp}})\\ \dot{\boldsymbol{\eta}}_e&=\frac{1}{2}(\boldsymbol{\eta}_e^{\times}\boldsymbol{\omega}_{bo}+\xi_e\boldsymbol{\omega}_{bo})\\ \dot{\xi}_e&=-\frac{1}{2}\boldsymbol{\omega}_{bo}^{T}\boldsymbol{\eta}_e\end{aligned} \tag{53}$$

The state vector for the system can be defined as

$$\boldsymbol{X}=[\xi_e-1,\boldsymbol{\eta}_e,\boldsymbol{\omega}_{bo},\tilde{\boldsymbol{\Theta}}]^T \tag{54}$$

To design the state feedback control and the adaptive law for $\hat{\boldsymbol{\Theta}}$ to drive the state vector to the condition $\boldsymbol{X}_0=[0,0,0,0]^T$, the following Lyapunov-candidate quadratic function is used:

$$\begin{aligned}V(\boldsymbol{X})=&\frac{1}{2}\boldsymbol{\omega}_{bo}^{T}\boldsymbol{J}\boldsymbol{\omega}_{bo}+\frac{1}{2}\tilde{\boldsymbol{\Theta}}^{T}\tilde{\boldsymbol{\Theta}}+k_q\boldsymbol{\eta}_e^{T}\boldsymbol{\eta}_e+k_q(\xi_e-1)^2\\ &+\cdots+\frac{1}{2}(K_J\boldsymbol{\omega}_{oi}^{T}\boldsymbol{\omega}_{oi}-\boldsymbol{\omega}_{oi}^{T}\boldsymbol{J}\boldsymbol{\omega}_{oi})\end{aligned} \tag{55}$$

where k_q is a positive constant, and $K_J\in\mathbb{R}$ is a constant such that

$$K_J>\lambda_{\max}(\boldsymbol{J}) \tag{56}$$

Because $\boldsymbol{J}$ is symmetric and positive definite, the following relationship holds:

$$\lambda_{\min}(\boldsymbol{J})\|\boldsymbol{\omega}_{oi}\|^2\le\boldsymbol{\omega}_{oi}^{T}\boldsymbol{J}\boldsymbol{\omega}_{oi}\le\lambda_{\max}(\boldsymbol{J})\|\boldsymbol{\omega}_{oi}\|^2 \tag{57}$$

Therefore, the last term in Eq. (55) satisfies

$$\frac{1}{2}(K_J\boldsymbol{\omega}_{oi}^{T}-\boldsymbol{\omega}_{oi}^{T}\boldsymbol{J}\boldsymbol{\omega}_{oi}\ge\frac{1}{2}(K_J-\lambda_{\max}(\boldsymbol{J}))\|\boldsymbol{\omega}_{oi}\|^2>0,\quad\forall\,\boldsymbol{\omega}_{oi}\in R^3$$

From here, it is easy to see that $V(\boldsymbol{X})$ defined in Eq. (55) is strictly positive for all $\boldsymbol{X}\neq\boldsymbol{X}_0$.

Taking the time derivative of $V(\boldsymbol{X})$ along the system's trajectory leads to

$$\dot{V}(t)=\boldsymbol{\omega}_{bo}^{T}J\dot{\boldsymbol{\omega}}_{bo}+\tilde{\boldsymbol{\Theta}}^{T}\tilde{\boldsymbol{\Theta}}+2k_q\boldsymbol{\eta}_e^{T}\dot{\boldsymbol{\eta}}_e+2k_q(\xi_e-1)\dot{\xi}-(\boldsymbol{\omega}_{oi})^{T}\boldsymbol{J}\dot{\boldsymbol{\omega}}_{oi} \tag{58}$$

where it has been taken into account that the magnitude of the vector angular velocity $\underline{\boldsymbol{\omega}}_{oi}$ of the orbital frame with respect to the inertial frame is a constant because of Hypothesis 1 and Eq. (3).

By using the first equation of Eqs. (53), Eq. (58) becomes

$$\begin{aligned}\dot{V}(t)=&\boldsymbol{\omega}_{bo}^{T}[\boldsymbol{J}(\boldsymbol{\omega}_{bo}^{\times}\boldsymbol{\omega}_{oi})-(\boldsymbol{\omega}_{bo}+\boldsymbol{\omega}_{oi})\times\boldsymbol{J}(\boldsymbol{\omega}_{bo}+\boldsymbol{\omega}_{oi})+\boldsymbol{\Phi}\boldsymbol{\Theta}\\ &+\boldsymbol{\tau}_t+\boldsymbol{\tau}_{\text{cp}}+\ldots\\ &\ldots+\tilde{\boldsymbol{\Theta}}^{T}\dot{\tilde{\boldsymbol{\Theta}}}+2k_q\boldsymbol{\eta}_e^{T}\dot{\boldsymbol{\eta}}_e+2k_q(\xi_e-1)\dot{\xi}_e-(\boldsymbol{\omega}_{oi})^{T}\boldsymbol{J}\dot{\boldsymbol{\omega}}\end{aligned} \tag{59}$$

By taking into account the Darboux equation, it yields

$$\begin{aligned}\dot{\boldsymbol{\omega}}_{oi}&=\frac{\mathrm{d}}{\mathrm{d}t}(\boldsymbol{R}_{b0}\boldsymbol{\omega}_{oi}^{o})=(\boldsymbol{R}_{b0}\boldsymbol{\omega}_{oi}^{o})=(R_{b0}\boldsymbol{\omega}_{oi}^{o})=-\boldsymbol{\omega}_{bo}^{\times}\boldsymbol{R}_{bo}\boldsymbol{\omega}_{oi}^{o}\\ &=-\boldsymbol{\omega}_{bo}^{\times}\boldsymbol{\omega}_{oi}\end{aligned} \tag{60}$$

Therefore, by considering Eq. (60) and the invariance of the scalar triple product to a circular per mutation of the terms, the third term of Eq. (59) becomes

$$\begin{aligned}-(\boldsymbol{\omega}_{oi})^{T}\boldsymbol{J}\dot{\boldsymbol{\omega}}_{oi}&=(\boldsymbol{\omega}_{oi})^{T}J(\boldsymbol{\omega}_{bo}^{\times}\boldsymbol{\omega}_{oi})=(\boldsymbol{J}\boldsymbol{\omega}_{oi})^{T}(\boldsymbol{\omega}_{bo}^{\times}\boldsymbol{\omega}_{oi})\\ &=\boldsymbol{\omega}_{bo}^{T}(\boldsymbol{\omega}_{bo}^{\times}\boldsymbol{J}\boldsymbol{\omega}_{oi})\end{aligned} \tag{61}$$

Furthermore, by taking into account that $\boldsymbol{\omega}_{bo}^{T}(\boldsymbol{\omega}_{bo}\times\bullet)=0$ for an arbitrary $\bullet\in\mathbb{R}^3$ and that the invariance of the scalar triple product is

$$\boldsymbol{\omega}_{bo}^{T}(\boldsymbol{\omega}_{bo}^{\times}\boldsymbol{J}\boldsymbol{\omega}_{bo})=(\boldsymbol{J}\boldsymbol{\omega}_{bo})^{T}(\boldsymbol{\omega}_{bo}^{\times}\boldsymbol{\omega}_{oi})=\boldsymbol{\omega}_{bo}^{T}\boldsymbol{J}(\boldsymbol{\omega}_{bo}^{\times}\boldsymbol{\omega}_{oi}) \tag{62}$$

the first term of Eq. (59) yields

$$\begin{aligned}&\boldsymbol{\omega}_{bo}^{T}[\boldsymbol{J}(\boldsymbol{\omega}_{bo}^{\times}\boldsymbol{\omega}_{oi})-(\boldsymbol{\omega}_{bo}+\boldsymbol{\omega}_{oi})\times\boldsymbol{J}(\boldsymbol{\omega}_{bo}+\boldsymbol{\omega}_{oi})+\boldsymbol{\Phi}\boldsymbol{\Theta}+\boldsymbol{\tau}_t+\boldsymbol{\tau}_{\text{cp}}=\ldots\\ &\ldots=\boldsymbol{\omega}_{bo}^{T}\boldsymbol{J}(\boldsymbol{\omega}_{bo}^{\times}\boldsymbol{\omega}_{oi})-\boldsymbol{\omega}T(\boldsymbol{\omega}_{oi}^{\times}\boldsymbol{J}\boldsymbol{\omega}_{bo})-\boldsymbol{\omega}_{bo}^{T}(\boldsymbol{\omega}_{oi}^{\times}\boldsymbol{J}\boldsymbol{\omega}_{oi})\\ &-\boldsymbol{\omega}_{bo}^{T}(\boldsymbol{\Phi}\boldsymbol{\Theta}+\boldsymbol{\tau}_t+\boldsymbol{\tau}_{\text{cp}})=\ldots\\ &\ldots=-\boldsymbol{\omega}_{bo}^{T}(\boldsymbol{\omega}_{oi}^{\times}\boldsymbol{J}\boldsymbol{\omega}_{oi})+\boldsymbol{\omega}_{bo}^{T}(\boldsymbol{\Phi}\boldsymbol{\Theta}+\boldsymbol{\tau}_t+\boldsymbol{\tau}_{\text{cp}})\end{aligned} \tag{63}$$

By substituting Eqs. (63) and (61) into Eq. (59), the time derivative of the Lyapunov function along the system trajectories becomes

$$\begin{aligned}\dot{V}(t)=&\boldsymbol{\omega}_{bo}^{T}(\boldsymbol{\Phi}\boldsymbol{\Theta})+\boldsymbol{\omega}_{bo}^{T}(\boldsymbol{\tau}_t+\boldsymbol{\tau}_{\text{cp}})+\boldsymbol{\Theta}T\dot{\tilde{\boldsymbol{\Theta}}}+2k_q\boldsymbol{\eta}_eT\dot{\boldsymbol{\eta}}_e\\ &+2k_q(\xi_e-1)\dot{\xi}_e\end{aligned} \tag{64}$$

Finally, by substituting Eq. (50) into Eq. (64) and rearranging the terms, it yields

$$\begin{aligned}\dot{V}(t)=&\boldsymbol{\omega}_{bo}^{T}\boldsymbol{\Phi}\hat{\boldsymbol{\Theta}}+\boldsymbol{\omega}_{bo}^{T}(\tau_t+\tau_{\text{cp}})\\ &+\tilde{\boldsymbol{\Theta}}^{T}(\boldsymbol{\Phi}^{T}\boldsymbol{\omega}_{bo}+\dot{\tilde{\boldsymbol{\Theta}}}+2k_q\boldsymbol{\eta}_e^{T}\dot{\boldsymbol{\eta}}_e+2k_q(\xi_e-1)\dot{\xi}_e\end{aligned} \tag{65}$$

Let the candidate adaptation law for the estimated parameter be

$$\dot{\hat{\boldsymbol{\Theta}}}=\boldsymbol{\Phi}^{T}\boldsymbol{\omega}_{bo} \tag{66}$$

and the candidate control law for the ideal control torque be

$$\boldsymbol{\tau}_t=-\boldsymbol{\tau}_{\text{cp}}-k_q\boldsymbol{\eta}_e-k_\omega\boldsymbol{\omega}_{bo}-\boldsymbol{\Phi}\hat{\boldsymbol{\Theta}} \tag{67}$$

where $k_\omega\in\mathbb{R}$ is a positive constant. Notably, this control law incorporates $\boldsymbol{\tau}_{\text{cp}}$, which depends on the known geometric properties of the satellites surfaces and on the current attitude of the spacecraft through the terms χ_i and δ_i [see Eq. (44)].

By substituting into Eq. (65) the expression of $\dot{\boldsymbol{\eta}}_e$ and $\dot{\xi}_e$ given by Eq. (13), of $\hat{\boldsymbol{\Theta}}$ given by Eq. (66), and of $\boldsymbol{\tau}_t$ given by Eq. (67), as well as by taking into account Eq. (51), it yields

$$\begin{aligned}\dot{V}(t)=&\boldsymbol{\omega}_{bo}^{T}(-k_q\boldsymbol{\eta}_e-k_\omega\boldsymbol{\omega}_{bo})+2\boldsymbol{\eta}_e^{T}\left(\frac{1}{2}k_q(\boldsymbol{\omega}_{bo}^{\times}\boldsymbol{\eta}_e+\xi_e\boldsymbol{\omega}_{bo})\right)\\ &+2k_q(\xi_eT-1)\left(-\frac{1}{2}\boldsymbol{\omega}_{bo}^{T}\boldsymbol{\eta}_e\right)\\ &=-k_q\boldsymbol{\omega}_{bo}^{T}\boldsymbol{\eta}e-k_\omega\boldsymbol{\omega}_{bo}^{T}\boldsymbol{\omega}_{bo}+k_q\boldsymbol{\eta}_e^{T}\xi_e\boldsymbol{\omega}_{bo}-k_q\xi_e\boldsymbol{\omega}_{bo}^{T}\boldsymbol{\eta}_e+k_q\boldsymbol{\omega}_{bo}^{T}\boldsymbol{\eta}_e\\ &=-k_\omega\boldsymbol{\omega}_{bo}^{T}\boldsymbol{\omega}_{bo}\end{aligned} \tag{68}$$

which is negative semidefinite for all values of $\boldsymbol{X}\neq0$ but not negative definite because it is $\dot{V}(t)=0$ for $\boldsymbol{\omega}_{bo}=0$ and any values of the variables that do not appear in the expression of $\dot{V}(t)$. Therefore, because of Lyapunov's stability theorem (theorem 4.1 in [36]), the equilibrium point $\boldsymbol{X}=0$ is stable.

To analyze the convergence properties, let us consider the closed set $\Omega=\{X\in\mathbb{R}^n|V(\boldsymbol{X})\le c\}$, for a generic $c>0$. Because $V(\boldsymbol{X})$ is radially unbounded (that is, $V(\boldsymbol{X})\to\infty$ as $\|\boldsymbol{X}\|\to\infty$), the set Ω is bounded for all positive c. Therefore, Ω is compact. Furthermore, as

$\dot{V}(\boldsymbol{X}) \leq 0$ for all $\boldsymbol{X} \in \Omega$, the set Ω is positively invariant. Therefore, all trajectories of the closed-loop system are bounded.

Moreover, by LaSalle's invariance principle (theorem 4.4 in [36]), all solutions starting in Ω will globally converge to the largest invariant set contained in the set E of all points in Ω where $\dot{V}(t) = 0$. Because of Eq. (68), E is the set of state variable values with $\boldsymbol{\omega}_{bo} = 0$, i.e.,

$$E \triangleq \{\dot{V}(t) = 0\} = \{\boldsymbol{X} \in \Omega | \dot{V}(\boldsymbol{\eta}_e, \xi_e - 1, \boldsymbol{\omega}_{bo}, \tilde{\boldsymbol{\Theta}}) = 0\} = \{\boldsymbol{X} \in \Omega | \boldsymbol{\omega}_{bo} = 0\} \tag{69}$$

The LaSalle invariance principle then ensures that

$$\lim_{t\to\infty} \boldsymbol{\omega}_{bo}(t) = 0$$

It now remains to analyze the system behavior in the largest invariant set contained in E. In set E, the closed-loop dynamics can be obtained by substituting the adaptation law of Eq. (66), the control law of Eq. (67), and the defining condition $\boldsymbol{\omega}_{bo} = 0$ of set E as given by Eq. (69) into the system dynamics equations [Eq. (53)], which lead to

$$\begin{aligned} 0 &= \boldsymbol{J}^{-1}(-\boldsymbol{\omega}_{oi}^{\times}\boldsymbol{J}\boldsymbol{\omega}_{oi} + \boldsymbol{\Phi}\tilde{\boldsymbol{\Theta}} - k_q\boldsymbol{\eta}_e) \\ \dot{\boldsymbol{\eta}}_e &= 0 \\ \dot{\xi}_e &= 0 \end{aligned} \tag{70}$$

The immediate solutions of the second and third equations of Eqs. (70) are $\boldsymbol{\eta}_e = \boldsymbol{\eta}_e'$ and $\xi_e = \xi_e'$, where $\boldsymbol{\eta}_e' \in \mathbb{R}^3$ contains three generic scalar constants and $\xi_e' \in \mathbb{R}$ is another generic scalar constant. Therefore, in set E, the spacecraft remains at rest with respect to the orbital coordinate system because the quaternion components are constant.

Furthermore, all of the terms within the parentheses in the first equation of Eq. (70) are constant. Indeed, besides the components of $\boldsymbol{\eta}_e$, the components of $\tilde{\boldsymbol{\Theta}}$ are also constant, as immediately results from Eqs. (51) and (66). Also, the term $\boldsymbol{\omega}_{oi}^{\times}\boldsymbol{J}\boldsymbol{\omega}_{oi}$ is constant, as $\boldsymbol{\omega}_{oi} = \boldsymbol{R}_{bo}\boldsymbol{\omega}_{oi}^{o}$ and $\boldsymbol{R}_{bo} = \boldsymbol{R}_{bo}(\boldsymbol{\eta}_e', \xi_e')$ is a constant matrix. Finally, in E, $\boldsymbol{\Phi}$ given by Eq. (49) is a constant matrix since in E the spacecraft attitude with respect to the orbital frame is constant.

Notably, the first equation of Eq. (70) implies that, in set E, the imaginary part of the quaternion can be written as

$$\boldsymbol{\eta}_e = \frac{1}{k_q}\boldsymbol{K}_e \tag{71}$$

where $\boldsymbol{K}_e \in \mathbb{R}^3$ contains three generic scalar constants. The constraint on the norm of the quaternion yields

$$\xi_e^2 = 1 - \left\| \frac{1}{k_q}\boldsymbol{K}_e \right\|^2 \tag{72}$$

Therefore, as $k_q \to \infty$, $\|\boldsymbol{\eta}_e\| \to 0$, and $\xi_e \to \pm 1$. In other words, as the constant gain k_q increases, $\boldsymbol{q}_e \to [0^T \pm 1]^T$: both of which solutions represent the condition of superposition of the body-fixed and the orbital coordinate systems (nadir-pointing orientation).

In conclusion, the adaptive control law [Eqs. (66) and (67)] ensures that all trajectories are globally bounded and that

$$\lim_{t\to\infty} \boldsymbol{\omega}_{bo}(t) = 0$$

and the final attitude error can be made arbitrarily small by choosing a sufficiently large k_q.

IV. Allocation of the Control Torque to the Actuators

As explained in Sec. II, the shifting masses can only generate a vectorial component of torque that lies on the plane perpendicular to the orbital velocity vector. Thus, when the satellite body-fixed coordinate is aligned with the orbital coordinate system, only the pitch and yaw axes can be controlled by moving the shifting masses positions, and no control torque is available about the roll axis. Therefore, additional actuators are needed in order to generate a vectorial component of the torque parallel to the orbital velocity vector and achieve a control torque vector spanning three dimensions. Two cases are here considered. In the first case, the shifting masses are augmented by one reaction wheel along the nominal roll axis. In the second case, the shifting masses are augmented by three magnetic torquers. In each of these two cases, the ideal control torque $\boldsymbol{\tau}_t$ can be allocated to the available actuators as determined here in the following.

From now on, the following hypothesis is considered holding:

Hypothesis 12: The spacecraft has a parallelepipedal shape (i.e., six flat faces).

A. Case 1: Control Allocation to Three Shifting Masses and One Reaction Wheel

We will now consider a spacecraft with three shifting masses and one reaction wheel. It is assumed that the three shifting masses have the same mass m_p and that they can translate along the three axes of the body-fixed coordinate system. The reaction wheel is considered as having its rotation axis aligned with the $\hat{\boldsymbol{x}}^b$ axis, as shown in Fig. 3. The positions of the three shifting masses can be represented by the following column matrix $\boldsymbol{r}_m \in \mathbb{R}^3$ having as elements the scalar distances of the shifting masses along their axis:

$$\boldsymbol{r}_m = \sum_{j=1}^{3} \boldsymbol{r}_j = \begin{bmatrix} r_x \\ 0 \\ 0 \end{bmatrix} + \begin{bmatrix} 0 \\ r_y \\ 0 \end{bmatrix} + \begin{bmatrix} 0 \\ 0 \\ r_z \end{bmatrix} \tag{73}$$

Consequently, the torque acting on the spacecraft due to the residual atmosphere is given by Eq. (46) with $p = 6$. The ideal control torque $\boldsymbol{\tau}_t$ given by the control law in Eq. (67) has to be allocated to the three shifting masses and the reaction wheel. Therefore, it is assumed to be

$$\underline{\boldsymbol{\tau}}_t = \underline{\boldsymbol{\tau}}_M + \underline{\boldsymbol{\tau}}_W \tag{74}$$

where the vector $\underline{\boldsymbol{\tau}}_W$ represents the torque provided by the reaction wheel.

Notably, the torque generated by the shifting masses $\underline{\boldsymbol{\tau}}_M$ shall always be confined to the plane perpendicular to the velocity vector $\underline{\hat{v}}_{s/c}$ in order to respect the existing physical constraint.

To obtain the expression of the torque generated by the reaction wheel, the angular momentum of the wheel needs to be taken into account The angular momentum of the wheel pertaining to the angular velocity of the spacecraft with respect to the inertial frame is

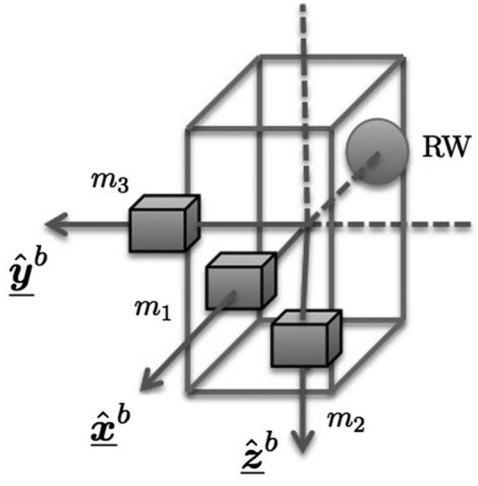

Fig. 3 Spacecraft system with three shifting masses and one reaction wheel.

assumed included in the term $\underline{\boldsymbol{\Gamma}}^A_{B^-}$: analogously to the common practice of modeling spacecraft with reaction wheels (see, for instance, [1]). Furthermore, the relative angular momentum of the wheel pertaining to the angular velocity of the wheel with respect to the spacecraft-fixed frame can be expressed as

$$\underline{\boldsymbol{\Gamma}}_W = J'/\underline{\boldsymbol{\Omega}} \tag{75}$$

where $J' \in \mathbb{R}$ is the moment of inertia of the wheel rotor about the rotation axis, and $\underline{\boldsymbol{\Omega}}$ is the angular velocity vector of the wheel rotor with respect to the spacecraft. Because the reaction wheel's rotation axis is aligned with the body axis $\underline{\hat{\boldsymbol{x}}}^b$, it is

$$\underline{\boldsymbol{\Omega}} = \Omega \underline{\hat{\boldsymbol{x}}}^b \tag{76}$$

By adding $\underline{\boldsymbol{\Gamma}}_W$ from Eq. (75) into the right-hand side of Eq. (22), by taking the time derivative, and by expressing all of the terms in components along the body-fixed coordinate system, the dynamic of the system with the reaction wheel can be written as

$$J\dot{\boldsymbol{\omega}} = -\dot{\boldsymbol{\omega}} \times \boldsymbol{J\omega} + \boldsymbol{\tau}_{\text{CM}} - + \boldsymbol{\tau}_M + \boldsymbol{\tau}_{\text{cp}} + \boldsymbol{\tau}_W \tag{77}$$

where the only difference with respect to Eq. (45) is the addition on the right-hand side of the column matrix $\boldsymbol{\tau}_W \in \mathbb{R}^3$ of components along the body-fixed coordinate system of the torque generated by the reaction wheel, which is composed by the wheel acceleration term and by the gyroscopic effect of the wheel angular momentum when moving attached to the spacecraft body at the same absolute angular velocity of the spacecraft and is expressed by

$$\boldsymbol{\tau}_W = -J'/\dot{\Omega}\underline{\hat{\boldsymbol{x}}}^b - \boldsymbol{\omega} \times J'\Omega\underline{\hat{\boldsymbol{x}}} \tag{78}$$

To achieve the control allocation of the ideal control torque $\underline{\boldsymbol{\tau}}_t$, it is convenient to decompose the ideal torque into the two vectorial components $\underline{\boldsymbol{\tau}}_{t_\perp}$ and $\underline{\boldsymbol{\tau}}_{t_\parallel}$, which are orthogonal and parallel, respectively, to the orbital velocity vector $\underline{\hat{\boldsymbol{v}}}_{\text{s/c}}$. Analogously, the reaction wheel torque $\underline{\boldsymbol{\tau}}_W$ is decomposed into $\underline{\boldsymbol{\tau}}_{W_\perp}$ and $\underline{\boldsymbol{\tau}}_{W_\parallel}$. The geometrical representation of torque decomposition is shown in Fig. 4.

By expressing all vectors in scalar components along the body-fixed coordinate system, it yields

$$\boldsymbol{\tau}_t = \boldsymbol{\tau}_{t_\perp} + \boldsymbol{\tau}_{t_\parallel}, \qquad \boldsymbol{\tau}_W = \boldsymbol{\tau}_{W_\perp} + \boldsymbol{\tau}_{W_\parallel} \tag{79}$$

with

$$\hat{\boldsymbol{v}}^T_{\text{s/c}}\boldsymbol{\tau}_{t_\perp} = 0, \qquad \hat{\boldsymbol{v}}^T_{\text{s/c}}\boldsymbol{\tau}_{W_\perp} = 0 \tag{80}$$

and

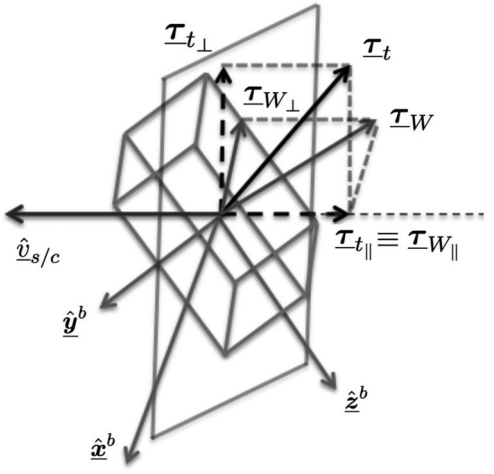

Fig. 4 Decomposition of the ideal control torque and the reaction wheel torque.

$$\hat{\boldsymbol{v}}^\times_{\text{s/c}}\boldsymbol{\tau}_{t_\parallel} = 0, \hat{\boldsymbol{v}}^\times_{\text{s/c}}\boldsymbol{\tau}_{W_\parallel} = 0 \tag{81}$$

By defining the projection operator

$$\boldsymbol{P}(\boldsymbol{q}_e) = [\boldsymbol{I}_{3\times 3} - \hat{\boldsymbol{v}}_{\text{s/c}}(\hat{\boldsymbol{v}}_{\text{s/c}})^T] \tag{82}$$

it yields, alternatively,

$$\boldsymbol{\tau}_{t_\perp} = \boldsymbol{P}(\boldsymbol{q}_e)\boldsymbol{\tau}_t, \qquad \boldsymbol{\tau}_{t_\parallel} = \hat{\boldsymbol{v}}_{\text{s/c}}(\hat{\boldsymbol{v}}^T_{\text{s/c}}\boldsymbol{\tau}_t) \tag{83}$$

and

$$\boldsymbol{\tau}_{W_\perp} = \boldsymbol{P}(\boldsymbol{q}_e)\boldsymbol{\tau}_W, \quad \text{and} \quad \boldsymbol{\tau}_{W_\parallel} = \hat{\boldsymbol{v}}_{\text{s/c}}(\hat{\boldsymbol{v}}^T_{\text{s/c}}\boldsymbol{\tau}_W) \tag{84}$$

The torque $\boldsymbol{\tau}_{t_\parallel}$ has to be allocated solely to the reaction wheel because the reaction wheel is the only actuator capable of generating a torque along the direction of the velocity (notably though, in general, although the reaction wheel is generating the component of torque parallel to $\boldsymbol{v}_{\text{s/c}}$, it is also generating a component perpendicular to it). Therefore, it yields

$$\boldsymbol{\tau}_{t_\parallel} = \boldsymbol{\tau}_{W_\parallel} \rightarrow \hat{\boldsymbol{v}}_{\text{s/c}}(\hat{\boldsymbol{v}}^T_{\text{s/c}}\boldsymbol{\tau}_t) = \hat{\boldsymbol{v}}_{\text{s/c}}(\hat{\boldsymbol{v}}^T_{\text{s/c}}\boldsymbol{\tau}_W) \rightarrow \hat{\boldsymbol{v}}^T_{\text{s/c}}\boldsymbol{\tau}_t = \hat{\boldsymbol{v}}^T_{\text{s/c}}\boldsymbol{\tau}_W \tag{85}$$

that, by taking into account Eq. (78), leads to

$$\hat{\boldsymbol{v}}^T_{\text{s/c}}\boldsymbol{\tau}_t = -J'/\dot{\Omega}\hat{v}^x_{\text{s/c}} - \omega_z J'/\Omega\hat{v}^y_{\text{s/c}} + \omega_y J'/\Omega\hat{v}^z_{\text{s/c}} \tag{86}$$

from which the wheel acceleration $\dot{\Omega}$ is obtained that is needed to generate the requested torque:

$$\dot{\Omega} = -\frac{1}{J'\hat{v}^x_{\text{s/c}}}((\hat{\boldsymbol{v}}^T_{\text{s/c}}\boldsymbol{\tau}_t) + \omega_z J'/\Omega\hat{v}^y_{\text{s/c}} - \omega_y J'\Omega\hat{v}^z_{\text{s/c}}) \tag{87}$$

By substituting Eq. (87) into Eq. (78), the reaction wheel torque required to generate the component of control torque parallel to the spacecraft velocity is given as a function of the angular velocity of the spacecraft with respect to the inertial frame, the spacecraft velocity vector, and the reaction wheel's angular velocity.

Once the torque $\boldsymbol{\tau}_W$ has been determined, the torque that the shifting masses need to generate is then given by $\boldsymbol{\tau}_M = \boldsymbol{\tau}_t - \boldsymbol{\tau}_W$. It can be shown that the torque $\boldsymbol{\tau}_M$ computed in this manner always belongs to the plane orthogonal to $\hat{\boldsymbol{v}}_{\text{s/c}}$. In fact,

$$\begin{aligned}\hat{\boldsymbol{v}}^T_{\text{s/c}}(\boldsymbol{\tau}_M) &= \hat{\boldsymbol{v}}^T_{\text{s/c}}(\boldsymbol{\tau}_t - \boldsymbol{\tau}_W) = \hat{\boldsymbol{v}}^T_{\text{s/c}}(\boldsymbol{\tau}_{t_\perp} + \boldsymbol{\tau}_{t_\parallel} - \boldsymbol{\tau}_{W_\perp} - \boldsymbol{\tau}_{W_{t_\parallel}}) \\ &= \hat{\boldsymbol{v}}^T_{\text{s/c}}(\boldsymbol{\tau}_{t_\perp} - \boldsymbol{\tau}_{W_\perp}) = 0\end{aligned} \tag{88}$$

This confirms that $\boldsymbol{\tau}_M$ is orthogonal to $\hat{v}^T_{\text{s/c}}\ \forall\ t$.

To steer the positions of the shifting masses identified by the column matrix $\boldsymbol{r}_m$, the torque $\boldsymbol{\tau}_M$ needs to be mapped to $\boldsymbol{r}_m$, according to the following equation, obtained by substituting Eq. (73) into the second equation of Eq. (46):

$$\boldsymbol{\tau}_M = -m_p \frac{K_{\text{CM}}}{M-}\hat{\boldsymbol{v}}^\times_{\text{s/c}}\boldsymbol{r}_m \tag{89}$$

Because the matrix $\hat{\boldsymbol{v}}_{\text{s/c}}(t)^\times$ is skew symmetric, and therefore singular, $\boldsymbol{r}_m$ cannot be directly found by inverting $\hat{\boldsymbol{v}}_{\text{s/c}}(t)^\times$ in solving Eq. (89). However, due to Eq. (88), the control torque $\boldsymbol{\tau}_M$ is guaranteed to be in the range space of $\hat{\boldsymbol{v}}_{\text{s/c}}(t)^\times$ for all t, so that Eq. (89) always has a solution for $\boldsymbol{r}_m$. Indeed, a solution is given by

$$\boldsymbol{r}_m = \frac{M - \boldsymbol{v}^\times_{\text{s/c}}\boldsymbol{\tau}_M}{\|\boldsymbol{v}_{\text{s/c}}\|^2 m_p K_{\text{CM}^-}} \tag{90}$$

In fact, by substituting Eq. (90) into Eq. (89), and by using the condition $\hat{\boldsymbol{v}}_{\mathrm{s/c}} \perp \boldsymbol{\tau}_M \ \forall\, t$ from Eq. (88) together with the property relating vector product to dot product $[\boldsymbol{a}^{\times}(\boldsymbol{b}^{\times \mathrm{c}}) = \boldsymbol{b}(\boldsymbol{a}^T\boldsymbol{c}) - \boldsymbol{c}(\boldsymbol{a}^T\boldsymbol{b})]$, it yields

$$\boldsymbol{\tau}_M = -m_p K_{\mathrm{CM}^-}\left(\frac{(\hat{\boldsymbol{v}}_{\mathrm{s/c}}^T\boldsymbol{\tau}_M)\boldsymbol{v}_{\mathrm{s/c}} - (\hat{\boldsymbol{v}}_{\mathrm{s/c}}^T\hat{\boldsymbol{v}}_{\mathrm{s/c}})\boldsymbol{\tau}_M}{\|\boldsymbol{v}_{s/c}\|^2 m_p K_{\mathrm{CM}^-}}\right) = \boldsymbol{\tau}_M \tag{91}$$

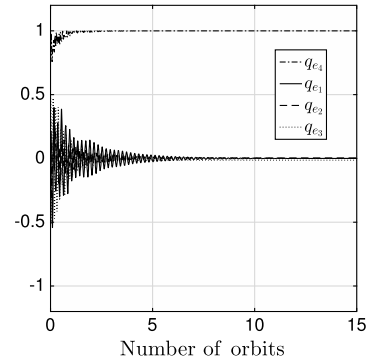

a) Attitude q_{e}

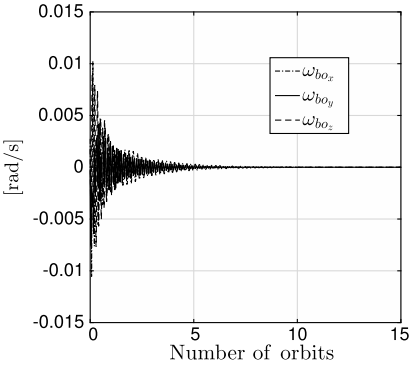

b) Angular velocity $\boldsymbol{\omega}_{\boldsymbol{bo}}$

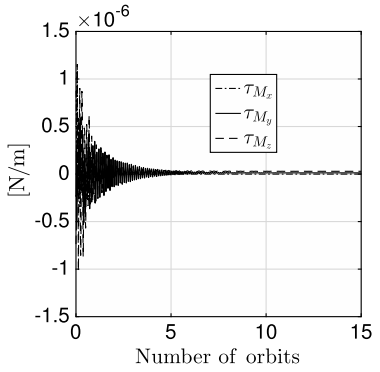

c) Shifting masses' torque output

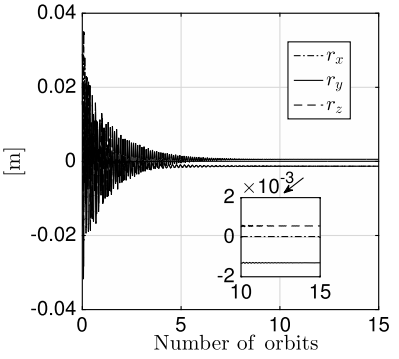

d) Shifting masses' positions

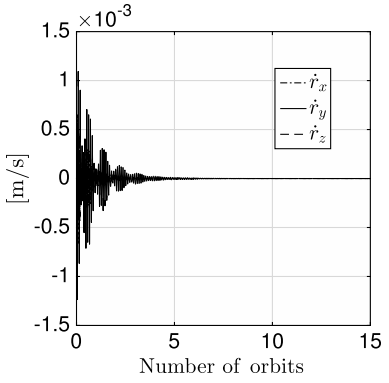

e) Shifting masses' speed

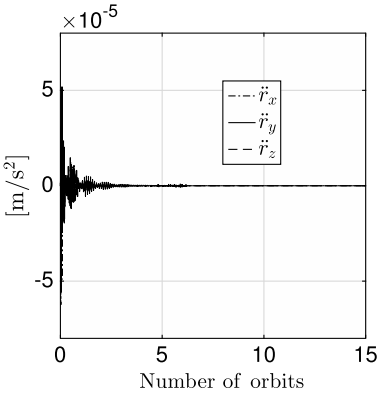

f) Shifting masses' accelerations

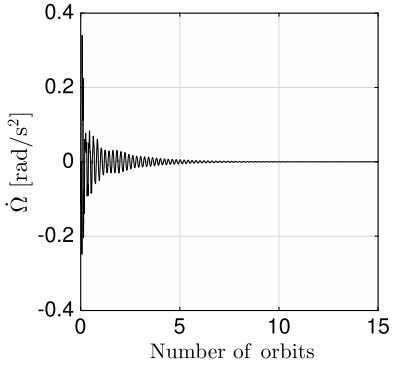

g) Reaction wheel's angular acceleration

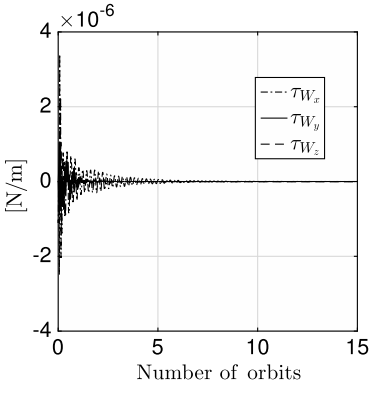

h) Reaction wheel's total torque

Fig. 5 Case 1: three-axis stabilization with three shifting masses and one reaction wheel.

B. Case 2: Control Allocation to Three Shifting Masses and Three Magnetic Torquers

In this section, the shifting masses control system is coupled with three magnetic torquers. The torque generated by magnetic actuators can be expressed as

$$\boldsymbol{\tau}_B = -\boldsymbol{B}^{\times} d \tag{92}$$

where $\boldsymbol{B}$ is the column matrix of scalar components in the body-fixed coordinate system of the local Earth's magnetic field, and $\boldsymbol{d}$ is the column matrix of the three magnetic dipole moments (assuming that the three magnetic torquers are mounted along the body-fixed coordinate system axes). The ideal control torque $\boldsymbol{\tau}_t$ given by the control law in Eq. (67) has to be allocated to the three shifting masses and the three magnetic torquers. Therefore, it is assumed to be

$$\underline{\boldsymbol{\tau}}_t = \underline{\boldsymbol{\tau}}_M + \underline{\boldsymbol{\tau}}_B \tag{93}$$

where the vector $\underline{\boldsymbol{\tau}}_B$ represents the torque provided by the magnetic torquers.

As a consequence of Eq. (92), the torque that can be generated by using magnetic actuators is always perpendicular to the Earth's magnetic field.

Nevertheless, with the exception of when the velocity of the spacecraft is parallel to the Earth's magnetic field, a three-dimensional torque can be generated by combining the torque generated by the magnetic torquers and by the shifting masses.

For the purpose of allocating the designed ideal torque to magnetic and shifting mass actuators, the control torque can be decomposed as follows:

$$\boldsymbol{\tau}_t = \boldsymbol{\tau}_{t_{\perp_B}} + \boldsymbol{\tau}_{t_{\parallel_B}}, \qquad \hat{\boldsymbol{B}}^T \tau_{t_{\perp_B}} = 0, \qquad \hat{\boldsymbol{B}}^{\times} \tau_{t_{\parallel_B}} = 0$$

Furthermore, the vector $\boldsymbol{\tau}_M$ can be decomposed as

$$\boldsymbol{\tau}_M = \boldsymbol{\tau}_{M_{\perp_B}} + \boldsymbol{\tau}_{M_{\parallel_B}}, \qquad \hat{\boldsymbol{B}}^T \boldsymbol{\tau}_{M_{\perp_B}} = 0, \qquad \hat{\boldsymbol{B}}^{\times} \boldsymbol{\tau}_{M_{\parallel_B}} = 0 \tag{94}$$

Because the three shifting masses are the only actuators that are able to generate a torque along the magnetic field, the scalar projection of $\boldsymbol{\tau}_M$ along the magnetic field must be identical to $\boldsymbol{\tau}_{t_{\parallel_B}}$. This condition leads to

$$\boldsymbol{\tau}_{M_{\parallel_B}} = \boldsymbol{\tau}_{t_{\parallel_B}} \Rightarrow (\boldsymbol{\tau}_M^T \hat{\boldsymbol{B}})\hat{\boldsymbol{B}} = (\boldsymbol{\tau}_t^T \hat{\boldsymbol{B}})\hat{\boldsymbol{B}} \rightarrow \boldsymbol{\tau}_M^T \hat{\boldsymbol{B}} = \boldsymbol{\tau}_t^T \hat{\boldsymbol{B}} \tag{95}$$

From Eq. (95), it is possible to find the following solution for $\boldsymbol{\tau}_M$, which also satisfies the requirement that $\boldsymbol{\tau}_M$ belongs to the plane orthogonal to $\hat{\boldsymbol{v}}_{\mathrm{s/c}}$:

$$\boldsymbol{\tau}_M \frac{\boldsymbol{\tau}_t^T \hat{\boldsymbol{B}}}{(\boldsymbol{P}(\boldsymbol{q}_e)\boldsymbol{\tau}_{t_{\parallel_B}})T\hat{\boldsymbol{B}}} (\boldsymbol{P}(\boldsymbol{q}e)\boldsymbol{\tau}_{t_{\parallel_B}}) \tag{96}$$

It is immediate to verify that the $\boldsymbol{\tau}_M$ given by Eq. (96) satisfies Eq. (95) and, for the property of the projection operator [see Eq. (82)], yields $\hat{\boldsymbol{v}}_{\mathrm{s/c}}^T \boldsymbol{\tau}_M = 0$.

Once $\boldsymbol{\tau}_M$ is found, the shifting masses position can be computed by using Eq. (90) as before.

Remark 1: Equation (96) has a singularity when $(\boldsymbol{P}(\boldsymbol{q}_e)\boldsymbol{\tau}_{\parallel B})\hat{\boldsymbol{B}} = 0$. This case appears only when the plane orthogonal to the velocity vector and the plane orthogonal to the magnetic field are aligned, i.e., $\hat{\boldsymbol{v}}_{\mathrm{s/c}} \equiv \hat{\boldsymbol{B}}$. In this case, from Eq. (96), $\|\boldsymbol{\tau}_M\| \rightarrow \infty$ that, because of Eq. (90) implies that $\|\boldsymbol{\tau}_m\| \rightarrow \infty$.

After $\boldsymbol{\tau}_M$ is computed, the magnetic torque can be determined by using Eq. (93) as

$$\boldsymbol{\tau}_B = \boldsymbol{\tau}_t - \frac{\boldsymbol{\tau}_t^T \hat{\boldsymbol{B}}}{(\boldsymbol{P}(\boldsymbol{q}_e)\boldsymbol{\tau}_{t_{\parallel_B}})^T \hat{\boldsymbol{B}}} (\boldsymbol{P}(\boldsymbol{q})\boldsymbol{\tau}_{t_{\parallel_B}}) \tag{97}$$

It is immediate to see $\boldsymbol{\tau}_B$ is always orthogonal to $\boldsymbol{B}$ as physically required because

$$\boldsymbol{B}^T \boldsymbol{\tau}_B = \boldsymbol{B}^T(\boldsymbol{\tau}_t - \boldsymbol{\tau}_M) = \boldsymbol{B}^T(\boldsymbol{\tau}_{t_{\perp_B}} - \boldsymbol{\tau}_{M_{\perp_B}}) = 0 \tag{98}$$

Once the control system computes the required control torque, the dipole $\boldsymbol{d}$ cannot be directly calculated by inverting the matrix $[-\boldsymbol{B}^{\times}]$ in Eq. (92) because $[-\boldsymbol{B}^{\times}]$ is always singular. However, due to the property in Eq. (98), the required magnetic control torque $\boldsymbol{\tau}_B$ is guaranteed to be in the range of $[-\boldsymbol{B}^{\times}]$ so that Eq. (92) always has a solution for $\boldsymbol{d}$. Indeed, a solution is given by

$$\boldsymbol{d} = \frac{\boldsymbol{B}^{\times} \boldsymbol{\tau}_B}{\|\boldsymbol{B}\|^2} \tag{99}$$

In fact, by substituting Eq. (99) into Eq. (92), and by using the condition $\hat{\boldsymbol{B}} \perp \boldsymbol{\tau}_B$, Eq. (98) yields

$$\boldsymbol{\tau}_B = -\left(\frac{\boldsymbol{B}^{\times}\boldsymbol{B}^{\times}\boldsymbol{\tau}_B}{\|\boldsymbol{B}\|^2}\right) = -\left(\frac{(\boldsymbol{B}^T\boldsymbol{\tau}_B)\boldsymbol{B} - (\boldsymbol{B}^T\boldsymbol{B})\boldsymbol{\tau}_B}{\|\boldsymbol{B}\|^2}\right) = \boldsymbol{\tau}_B \tag{100}$$

C. Control Saturation

By scaling the ideal control torque using the following rule:

$$\boldsymbol{\tau}_t \begin{cases} \boldsymbol{\tau}_t, & \|\boldsymbol{r}_m\|_{\infty} \leq r_{\max} \\ \dfrac{r_{\max}}{\|\boldsymbol{r}_m\|_{\infty}} \boldsymbol{\tau}_t, & \|\boldsymbol{r}_m\|_{\infty} > r_{\max} \end{cases} \tag{101}$$

where $r_{\max}$ is the maximum linear displacement of each of the shifting masses and $\|\boldsymbol{r}_m\|_{\infty} = \max\{r_1, r_2, r_3\}$, it is ensured that the shifting masses can generate the requested torque.

V. Numerical Experiments

In this section, the results of numerical simulations are presented for the two attitude control methods introduced in previous sections. The scenario used for these simulations considers a 30 by 10 by 10 cm spacecraft (three-unit CubeSat) with a total mass $M = 4.2$ kg. The spacecraft is equipped with three shifting masses, all of equal mass $m_p = 0.3$ kg. The spacecraft has an inertia matrix $\boldsymbol{J} = \mathrm{diag}[0.032, 0.0416, 0.013]\ \mathrm{kg \cdot m^2}$, and $\boldsymbol{r} = [2\ 2\ 2]^T \cdot 10^{-3}$ m. The spacecraft's orbital altitude is $h = 350$ km and its inclination is $i = 88$ deg. The orbital period is $T_o = 5492.1$ s. The initial quaternion and angular velocity with respect to the orbital

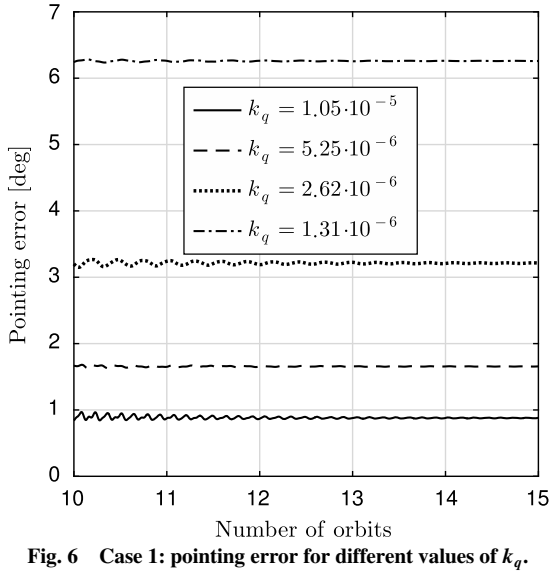

Fig. 6 Case 1: pointing error for different values of k_q.

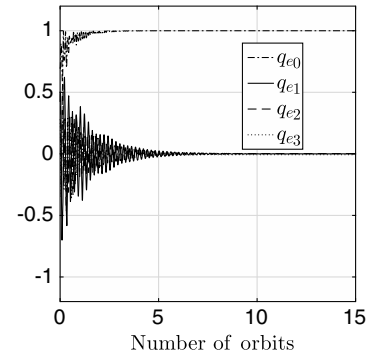

a) Attitude q_e

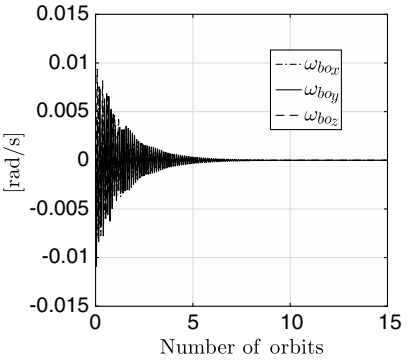

b) Angular velocity ω_{bo}

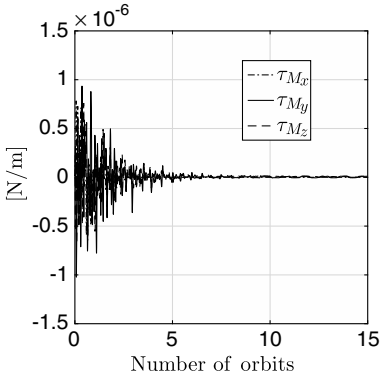

c) Shifting masses' torque output

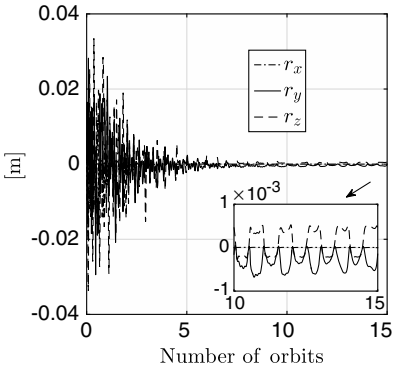

d) Shifting masses' positions

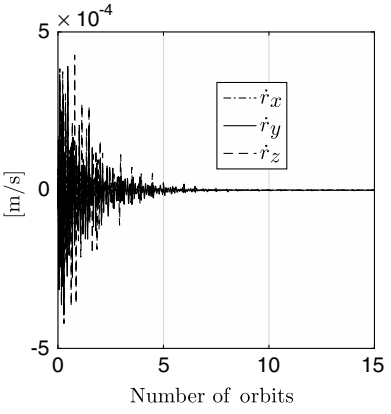

e) Shifting masses' speed

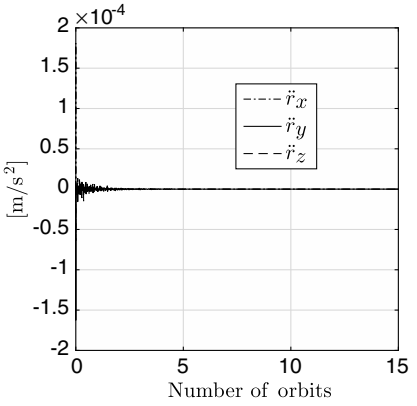

f) Shifting masses' accelerations

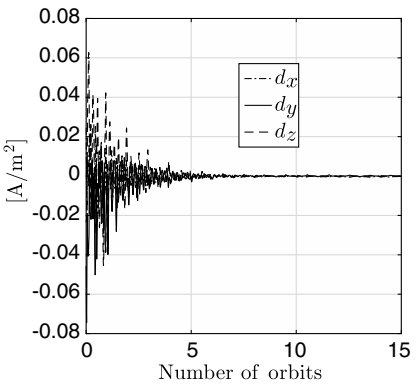

g) Magnetic torquers' dipole

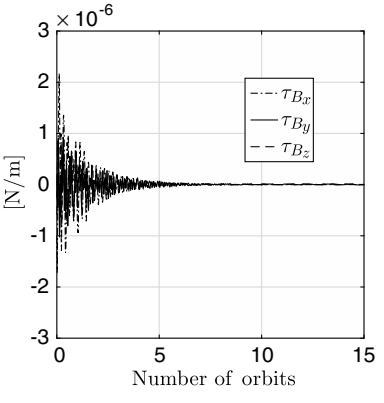

h) Magnetic torquers's torque

Fig. 7 Case 2: three-axis stabilization with three shifting masses and three magnetic torquers.

coordinate system are $\boldsymbol{q}_e = [0.812 \quad 0.178 \quad 0.301 \quad 0.467]^T$, and $\boldsymbol{\omega}_{bo} = [2.741 \ -0.4 \ 1.735]^T \cdot 10{-}3$ rad/s, respectively. The feedback control gains are $k_q = 1.05 \cdot 10^{-5}$ and $k_\omega = 1.5 \cdot 10^{-5}$. The simulations were performed in MATLAB® and Simulink® R2012b. The numerical integrator used was the fourth-order Runge–Kutta with a fixed time step of $T_s = 0.01$ s.

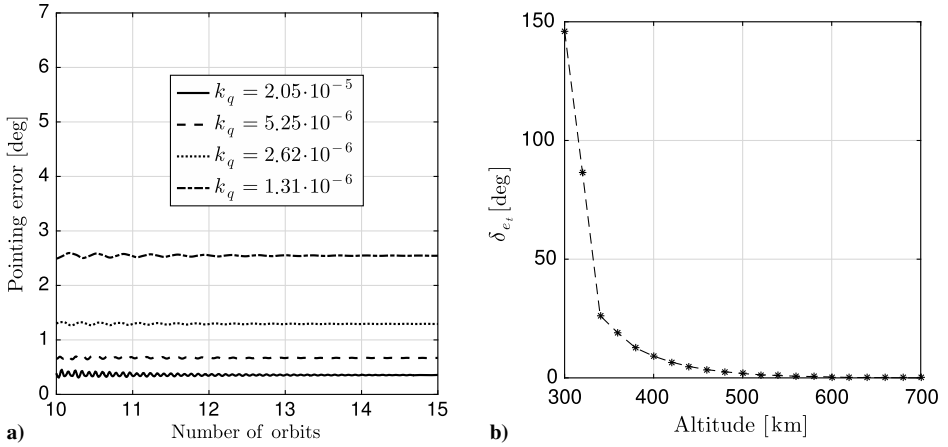

Fig. 8 Case 2: a) pointing error for different values of k_q, and b) performance comparison (difference in the residual maximum pointing error) between a magnetic control with only magnetic torquers and the one of case 2 including shifting masses and magnetic control.

A. Simulation Results: Case 1: Spacecraft with Three Shifting Masses and One Reaction Wheel

For these simulations, one reaction wheel is considered present along the x axis of the body-fixed coordinate system with $J' = 1 \cdot 10^{-5}$ kg $\cdot$ m^2. The simulations results of the numerical simulations performed for the three-axis stabilization are shown in Fig. 5. In particular, the plots of the attitude and angular velocity, reported in Figs. 5a and 5b, show that the system is able to successfully achieve three-axis stabilization in less than 15 orbits under the control laws in Eqs. (87) and (90). In particular, as shown analytically in Sec. III, $\boldsymbol{\omega}_{bo} \to 0$, and $\boldsymbol{q}_e \to [0, 1]^T$.

The torque output due to the shifting of the masses is represented in Fig. 5c, whereas the positions of the masses during the maneuver are shown in Fig. 5d. During the maneuver, all the three masses change their positions in order to generate the required torque. As expected, once the system has achieved the required attitude, the m_x mass stays at the origin because it cannot generate a torque because the x axis is aligned with the velocity vector and the cross product between the velocity vector and the vector representing the position of the m_x mass is zero. The masses m_y and m_z converge to a constant position such that they compensate for the constant torque generated by the position of CM$^-$. For this reason, both the velocities and linear acceleration of the shifting masses converge to zero, as shown in Figs. 5e and 5f, respectively.

Figures 5g and 5h show that the reaction wheel generates a torque only during the maneuvering. When the system is aligned with the required attitude, the aerodynamic drag does not generate a torque along the roll axis. Thus, the reaction wheel is not used to compensate any torque along this direction; consequently, $\dot{\Omega} \to 0$.

In Sec. III, it has been proved analytically that the final attitude error can be made arbitrarily small by increasing the value of k_q. This conclusion is confirmed by the simulation results presented in Fig. 6, where the time history of the final attitude error is shown for four different values of k_q. The scalar representing the final attitude error in Fig. 6 is defined as the square root of the sum of the squares of the roll, pitch, and yaw angle errors. It is evident that the final attitude error decreases as the value of k_q increases.

B. Simulation Results: Case 2: Spacecraft with Three Shifting Masses and Three Magnetic Torquers

In the numerical simulations reported in this section, the spacecraft is considered equipped with three shifting masses and three orthogonal magnetic torquers. The physical parameters and initial conditions used in these simulations are the same as in the previous section.

As shown in Figs. 7a and 7b, the spacecraft is able to achieve the required orientation in less than 15 orbits, and $\boldsymbol{\omega}_{bo} \to 0$, and $\boldsymbol{q}_e \to [0^T, 1]^T$. Figures 7c and 7d show the time history of the shifting masses torque output and positions. Also, in this case during the stabilization, all the shifting masses change their positions in order to stabilize the satellite. Once the stabilization is achieved, the shifting mass m_x does not move because no torque can be generated by moving the shifting mass along the direction of the velocity vector. Instead, the other two masses (m_y and m_z) that are orthogonal to the velocity vector keep on oscillating, even when the satellite has achieved the required orientation. This is due to the fact that the direction of the Earth's orbital magnetic field in the body-fixed coordinate system changes during the orbit. Therefore, the allocation of the required torque between the magnetic actuators and the shifting masses keep changing (see Figs. 7e–7h). As is shown in Fig. 8a, the residual errors on pitch, roll, and yaw angle all converge to small constants; in accordance with the analysis in Sec. III, the constant residual errors can be made smaller by increasing k_q.

The advantage of adding shifting masses to magnetic torquers is particularly evident at lower altitude. Figure 8b shows a comparison between a standard magnetic control and shifting masses plus magnetic control. To compare the performance of the two methods at various altitudes, the difference in the final attitude error has been evaluated as

$$\delta_{e_t} = \delta_{e_1} - \delta_{e_2}$$

where $\delta_{e_1} = \sqrt{\phi_{e_1}^2 \theta_{e_1}^2 + \psi_{e_1}^2}$ refers to the final attitude error with a standard magnetic control only, and $\delta_{e_2} = \sqrt{\phi_{e_2}^2 \theta_{e_2}^2 + \psi_{e_2}^2}$ refers to the final attitude error with magnetic control plus shifting masses. As shown in Fig. 8b, the use of shifting masses largely reduces the attitude error at lower altitudes. At higher altitudes, the atmospheric density decreases; consequently, the effect of the aerodynamic torque decreases. At altitudes greater then 600 km, according to the simulations, there is no improvement with respect to the standard magnetic attitude control.

VI. Conclusions

In this paper, a method is presented of using shifting masses to achieve three-axis stabilization by variating the aerodynamic torque.

Because the torque generated by shifting masses is constrained on a plane perpendicular to the orbital velocity vector, an additional set of actuators (either one reaction wheel or three magnetic torquers) is considered to achieve full actuation.

To design a control algorithm that achieves three-axis stabilization, a two-step process is used. First, an ideal control torque is designed based on an adaptive nonlinear feedback control. The stability of the closed-loop system is demonstrated through a Lyapunov method, and its convergence is analyzed through LaSalle's invariance principle. In the second step, the designed ideal torque is allocated to three shifting masses and to either one reaction wheel or three magnetic torquers.

The control allocation algorithm ensures that the torque assigned to different actuators can be physically generated.

The performance of the proposed method is demonstrated through numerical simulations. In particular, we consider a spacecraft on a circular orbit at 350 km of altitude, where the major disturbance torque is typically the aerodynamic drag. The spacecraft needs to perform a three-axis stabilization beginning from a generic orientation. Two numerical examples are presented: one using three shifting masses and one reaction wheel, and the other using three shifting masses and three magnetic torquers. In both cases, the numerical simulation results confirm the analytic results regarding the stability and convergence of the proposed control law.

The proposed method to exploit the residual aerodynamic torque to control a spacecraft is particularly advantageous for small spacecraft (e.g., nanosatellites), where the limited power, size, and inertia restrict the ability of the attitude control system to overcome the external disturbances torques. Notably, the proposed use of shifting masses coupled with magnetic control greatly decreases the residual oscillation error due to underactuation typically associated with the magnetic-controlled attitude of small spacecraft in the presence of residual aerodynamic torque [6,43–48]. Therefore, using center-of-mass shifting in combination with magnetic control might enable higher pointing accuracy for three-axis stabilization of small spacecraft in low Earth orbit.

References

[1] Wie, B., *Space Vehicle Dynamics and Control*, 2nd ed., AIAA, Reston, VA, 2008, pp. 36–40, 365–374, 451–456.

[2] Silani, E., and Lovera, M., "Magnetic Spacecraft Attitude Control: A Survey and Some New Results," *Control Engineering Practice*, Vol. 13, No. 3, 2005, pp. 357–371.

[3] Hughes, P. C., *Spacecraft Attitude Dynamics*, Wiley, New York, 1986, pp. 217–225.

[4] Kumar, R. R., Mazanek, D. D., and Heck, M. L., "Simulation and Shuttle Hitchhiker Validation of Passive Satellite Aerostabilization," *Journal of Spacecraft and Rockets*, Vol. 32, No. 5, 1995, pp. 806–811.

[5] Kumar, R. R., Mazanek, D. D., and Heck, M. L., "Parametric and Classical Resonance in Passive Satellite Aerostabilization," *Journal of Spacecraft and Rockets*, Vol. 33, No. 2, 1996, pp. 228–234.

[6] Psiaki, M. L., "Nanosatellite Attitude Stabilization Using Passive Aerodynamics and Active Magnetic Torquing," *Journal of Guidance, Control, and Dynamics*, Vol. 27, No. 3, 2004, pp. 347–355.

[7] Virgili Llop, J., "Aerostability for Low Altitude Flying CubeSats," *2nd IAA Conference on University Satellites Missions and Cubesat Workshop*, IAA Paper IAA-CU-13-10-03, Feb. 2013.

[8] Virgili Llop, J., Roberts, P. C. E., and Hao, Z., "Aerodynamic Attitude and Orbit Control Capabilities of the DDSAT CubeSat," *37th Annual AAS Rocky Mountain Section Guidance and Control Conference*, Vol. 14, AAS, Univelt, San Diego, CA, 2014, pp. 321–333.

[9] Leonard, C. L., Hollister, W. M., and Bergmann, E. V., "Orbital Formationkeeping with Differential Drag," *Journal of Guidance, Control, and Dynamics*, Vol. 12, No. 1, 1989, pp. 108–113.

[10] Palmerini, G. B., Sgubini, S., and Taini, G., "Spacecraft Orbit Control Using Air Drag," *56th International Astronautical Congress of the International Astronautical Federation, the International Academy of Astronautics, and the International Institute of Space Law*, IAC Paper IAC-05-C1.6.10, 2005.

[11] Bevilacqua, R., and Romano, M., "Rendezvous Maneuvers of Multiple Spacecraft Using Differential Drag Under J2 Perturbation," *Journal of Guidance, Control, and Dynamics*, Vol. 31, No. 6, 2008, pp. 1595–1607.

[12] Bevilacqua, R., Hall, J., and Romano, M., "Multiple Spacecraft Docking Maneuvers by Differential Drag and Low Thrust Engines," *Celestial Mechanics and Dynamical Astronomy*, Vol. 106, No. 1, 2010, pp. 69–88.

[13] Varma, S., and Kumar, K. D., "Multiple Satellite Formation Flying Using Differential Aerodynamic Drag," *Journal of Spacecraft and Rockets*, Vol. 49, No. 2, 2012, pp. 325–336.

[14] Harris, M. W., and Açıkmeşe, B., "Minimum Time Rendezvous of Multiple Spacecraft Using Differential Drag," *Journal of Guidance, Control, and Dynamics*, Vol. 37, No. 2, 2014, pp. 365–373.

[15] Virgili Llop, J., Roberts, P. C. E., Palmer, K., Hobbs, S., and Kingston, J., "Descending Sun-Synchronous Orbits with Aerodynamic Inclination Correction," *Journal of Guidance, Control, and Dynamics*, Vol. 38, No. 5, 2015, pp. 831–842.

[16] Virgili Llop, J., Roberts, P. C. E., and Hara, N. C., "Atmospheric Interface Reentry Point Targeting Using Aerodynamic Drag Control," *Journal of Guidance, Control, and Dynamics*, Vol. 38, No. 3, 2015, pp. 403–413.

[17] Pastorelli, M., Bevilacqua, R., and Pastorelli, S., "Differential-Drag-Based Roto-Translational Control for Propellant-Less Spacecraft," *Acta Astronautica*, Vol. 114, Sept.–Oct. 2015, pp. 6–21.

[18] Grubin, C. D., "Dynamics of a Vehicle Containing Moving Parts," *Journal of Applied Mechanics*, Vol. 29, No. 3, 1962, pp. 486–488.

[19] Woolsey, C. A., "Reduced Hamiltonian Dynamics for a Rigid Body/Mass Particle System," *Journal of Guidance, Control, and Dynamics*, Vol. 28, No. 1, 2005, pp. 131–138.

[20] Ross, I. M., "Mechanism for Precision Orbit Control with Applications to Formation Keeping," *Journal of Guidance, Control, and Dynamics*, Vol. 25, No. 4, 2002, pp. 818–820.

[21] Thomas, S., Paluszek, M., Wie, B., and Murphy, D., "Design and Simulation of Sailcraft Attitude Control Systems Using the Solar Sail Control Toolbox," *AIAA Guidance, Navigation, and Control Conference and Exhibit*, AIAA Paper 2004-4890, 2004.

[22] Wie, B., "Solar Sail Attitude Control and Dynamics, Part 1," *Journal of Guidance, Control, and Dynamics*, Vol. 27, No. 4, 2004, pp. 526–535.

[23] Wie, B., "Solar Sail Attitude Control and Dynamics, Part Two," *Journal of Guidance, Control, and Dynamics*, Vol. 27, No. 4, 2004, pp. 536–544.

[24] Wie, B., and Murphy, D., "Solar-Sail Attitude Control Design for a Flight Validation Mission," *Journal of Spacecraft and Rockets*, Vol. 44, No. 4, 2007, pp. 809–821.

[25] Hamidi-Hashemi, H., "Liapunov Analysis of a Two Dimensional Unconstrained Particle Motion in a Rigid Body Spinning About the Thrust Axis," *Proceedings of the 36th Midwest Symposium on Circuits and Systems*, Vol. 2, IEEE, New York, Aug. 1993, pp. 971–973.

[26] Edwards, T. L., and Kaplan, M. H., "Automatic Spacecraft Detumbling by Internal Mass Motion," *AIAA Journal*, Vol. 12, No. 4, 1974, pp. 496–502.

[27] Kunciw, B., and Kaplan, M., "Optimal Space Station Detumbling by Internal Mass Motion," *Automatica*, Vol. 12, No. 5, 1976, pp. 417–425.

[28] Guo, P., and Zhao, L., "Modeling and Attitude Control of a Spinning Spacecraft with Internal Moving Mass," *Advanced Materials Research*, Vols. 760–762, Sept. 2013, pp. 1216–1220.

[29] Halsmer, D. M., and Mingori, D. L., "Nutational Stability and Passive Control of Spinning Rockets with Internal Mass Motion," *Journal of Guidance, Control, and Dynamics*, Vol. 18, No. 5, 1995, pp. 1197–1203.

[30] Yam, Y., Mingori, D. L., and Halsmer, D. M., "Stability of a Spinning Axisymmetric Rocket with Dissipative Internal Mass Motion," *Journal of Guidance, Control, and Dynamics*, Vol. 20, No. 2, 1997, pp. 306–312.

[31] Hervas, J., Reyhanoglu, M., and Tang, H., "Thrust-Vector Control of a Three-Axis Stabilized Spacecraft with Fuel Slosh Dynamics," *13th International Conference on Control, Automation and Systems (ICCAS)*, IEEE, New York, Oct. 2013, pp. 761–766.

[32] Kumar, K., and Zou, A. M., "Attitude Control of Miniature Satellites Using Movable Masses," *SpaceOps 2010 Conference*, AIAA Paper 2010-1982, April 2010.

[33] Atkins, B. M., and Henderson, T. A., "Under-Actuated Moving Mass Attitude Control for a 3U Cubesat Mission," *Advances in the Astronautical Sciences*, Vol. 143, July 2012, pp. 2083–2094.

[34] Petsopoulos, T., Regan, F. J., and Barlow, J., "Moving-Mass Roll Control System for Fixed-Trim Re-Entry Vehicle," *Journal of Spacecraft and Rockets*, Vol. 33, No. 1, 1996, pp. 56–60.

[35] Atkins, B. M., and Queen, E. M., "Internal Moving Mass Actuator Control for Mars Entry Guidance," *Journal of Spacecraft and Rockets*, Vol. 52, No. 5, 2015, pp. 1294–1310.

[36] Khalil, H., *Nonlinear Systems*, 3rd ed., Prentice–Hall, Upper Saddle River, NJ, Jan. 2002, pp. 126–132.

[37] Selva, D., and Krejci, D., "A Survey and Assessment of the Capabilities of Cube-Sats for Earth Observation," *Acta Astronautica*, Vol. 74, May–June 2012, pp. 50–68.

[38] Wisniewski, R., "Linear Time-Varying Approach to Satellite Attitude Control Using Only Electromagnetic Actuation," *Journal of Guidance, Control, and Dynamics*, Vol. 23, No. 4, 2000, pp. 640–647.

[39] Liang, J., Fullmer, R., and Chen, Y., "Time-Optimal Magnetic Attitude Control for Small Spacecraft," *43rd IEEE Conference on Decision and Control*, Vol. 1, IEEE Publ., Piscataway, NJ, 2004, pp. 255–260.

[40] Psiaki, M. L., "Magnetic Torquer Attitude Control via Asymptotic Periodic Linear Quadratic Regulation," *Journal of Guidance, Control, and Dynamics*, Vol. 24, No. 2, 2001, pp. 386–394.

[41] Lovera, M., De Marchi, E., and Bittanti, S., "Periodic Attitude Control Techniques for Small Satellites with Magnetic Actuators," *IEEE Transactions on Control Systems Technology*, Vol. 10, No. 1, 2002, pp. 90–95.

[42] Lovera, M., and Astolfi, A., "Spacecraft Attitude Control Using Magnetic Actuators," *Automatica*, Vol. 40, No. 8, 2004, pp. 1405–1414.
[43] Mayer, G., "Design and Global Analysis of Spacecraft Attitude Control Systems," NASA Ames Research Center TR R-361, Moffett Field, CA, March 1971.
[44] Haug, E. J., *Computer Aided Kinematics and Dynamics of Mechanical Systems, Vol. 1: Basic Methods*, Allyn and Bacon, Needham Heights, MA, 1989, pp. 317–335.
[45] Likins, P., *Elements of Engineering Mechanics*, International Student ed., McGraw–Hill, New York, 1973, p. 409.
[46] Wertz, J. R., *Spacecraft Attitude Determination and Control*, Vol. 73, Astrophysics and Space Science Library, D. Reidel Publishing, Dordrecht, The Netherlands, 1978, pp. 573–575.
[47] "U.S. Standard Atmosphere, 1976" U.S. Committee on Extension to the Standard Atmosphere, National Oceanic and Atmospheric Administration Rept. NOAA-S/T 76-1562, Washington, D.C., 1976, pp. 50–97.
[48] Chesi, S., Gong, Q., Pellegrini, V., Cristi, R., and Romano, M., "Automatic Mass Balancing of a Spacecraft Three-Axis Simulator: Analysis and Experimentation," *Journal of Guidance, Control, and Dynamics*, Vol. 37, No. 1, 2013, pp. 197–206.